Title
Nonlinear Dynamic Analyses of Perris Dam Using Transition Probability to Model Interbedded Alluvial Strata

Journal
Journal of Geotechnical and Geoenvironmental Engineering, 148(1)

ISSN
1090-0241

Authors
Paull, Nicholas A
Boulanger, Ross W
DeJong, Jason T
et al.

Publication Date
2022

DOI
10.1061/(asce)gt.1943-5606.0002663

Peer reviewed

Nonlinear dynamic analyses of Perris Dam using transition probability to model interbedded alluvial strata

By

Nicholas A. Paull, Ph.D., A.M.ASCE
Corresponding Author: Project Engineer, GEI Consultants Inc.,
Rancho Cordova, CA 95670, npaull@geiconsultants.com

Ross W. Boulanger, Ph.D., P.E., F.ASCE
Professor, Department of Civil and Environmental Engineering,
University of California, Davis, CA 95616, rwboulanger@ucdavis.edu

Jason T. DeJong, Ph.D., M.ASCE
Professor, Department of Civil and Environmental Engineering,
University of California, Davis, CA 95616, jdejong@ucdavis.edu

Steven J. Friesen, P.E.
Senior Engineer, California Department of Water Resources
Sacramento, California, USA, Steven.Friesen@water.ca.gov

ASCE Journal of Geotechnical & Geoenvironmental Engineering (in press)
Authors' final copy
2021

Abstract

This case study presents an application of a conditional transition probability method for interpreting subsurface stratigraphy for the interbedded alluvium underlying Perris Dam and evaluating the effects of stratigraphic uncertainty on nonlinear dynamic analysis (NDA) results for design earthquake loading. The challenges involved in synthesizing information from different sources (i.e., geologic conditions, different site investigation tools, lab data, field classifications) into soil categories for interbedded alluvium are examined. The application of conditional transition probability methods for developing three-dimensional (3D) realizations of the upper Holocene and lower Pleistocene alluvial strata over a 305 m wide interval along the dam alignment is described including the challenges with insufficient data and limitations involved with utilizing a stationary, geostatistical method for approximating nonstationary geologic conditions. Two-dimensional (2D) NDA models of Perris Dam are created by slicing the 3D transition probability realizations into five 2D cross sections. The constitutive models PM4Sand and PM4Silt were used to model the sand and clay soil categories in the alluvial strata, as well as the different zones in the embankment. The deformations and variability in deformations for each cross section are compared, and sensitivity studies are completed to examine the impact of several factors including the impacts of the small strain shear modulus for the alluvium, the mean lengths and sills for the alluvium categories, the strengths for each alluvium soil category, and different ground motions. NDA cross sections of Perris Dam with uniformly (non-categorical) distributed properties are performed with and without additional deterministic embedded soil lenses and the deformations are compared with the transition probability models and deterministic models previously completed by others. The use of the conditional transition probability models for NDAs of Perris Dam, along with the implications and lessons for practice, are discussed.

Introduction

Alluvial and fluvial environments, on which many embankment dams and levees are founded, are often comprised of interbedded soils that range significantly in their soil properties and dynamic behaviors. Interbedded soils are often idealized into discrete groups based on perceived connectivity in site investigation data (i.e., fence diagrams) to model these variations in seismic evaluations of embankment dams. When used in nonlinear dynamic analyses (NDAs), the assumptions made in specifying the extents of these groups may significantly impact the computed deformations.

The use of geostatistical tools to investigate the effects of geological uncertainty in limit equilibrium or deformation (finite difference or finite element) analyses can generally be separated into two categories; (1) using conditional or unconditional random fields to consider the uncertainty of continuous soil property variations within a single soil category or (2) using transition probability methods to consider stratigraphic differences in discrete soil categories. Liu et al. (2017) provide a summary of twenty limit equilibrium studies using conditional and unconditional random fields of soil properties. The greatest benefits from directly conditioning the models to site investigation data in many of these studies were for cases that had correlation lengths around 0.5 to 2 times the base length of the geotechnical system. None of these studies considered NDAs for seismic stability or deformations involving liquefaction effects. Paull et al. (2020a) used unconditional random fields to stochastically model the spatial variability of corrected Standard Penetration Test (SPT) $(N_1)_{60cs}$ values in a non-interbedded foundation stratum beneath embankments with heights of 5 m to 45 m, and determined that uniform analysis models should use the 45th - 50th percentile $(N_1)_{60cs}$ in the foundation stratum to obtain median deformations and the 30th percentile $(N_1)_{60cs}$ to obtain conservative deformations. The latter finding was similar to recommendations based on results for a 45 m high embankment dam completed by Boulanger and Montgomery (2016). Paull et al. (2020b) examined the use of conditional random fields of $(N_1)_{60cs}$ in a non-interbedded foundation stratum for embankment dams and suggested that conditional simulations do not significantly decrease the variability of estimated deformations from NDAs unless there are greater than three borings spaced closer than the scale of fluctuation within the foundation stratum. The above are consistent with the general findings from prior studies that examined the use of random field methods for representing soil variability in analyses of various geotechnical systems to different loadings (e.g., Joint TC205/TC304 Working Group 2017).

Transition probability geostatistics for categorical variables based on Markov chains (e.g., Carle and Fogg 1997) have been used extensively in hydrogeology studies and to a lesser degree in geotechnical stability or deformation analyses. Langousis et al. (2018) discuss the advantages of Markov based transition probability geostatistics relative to more traditional geostatistical methods and the limitations and epistemic uncertainties that arise from its underlying assumptions for hydrogeology applications. Li et al. (2016) applied a Markov based transition probability method to generate realizations for finite element slope stability analyses using the strength reduction method. Krage et al. (2016) evaluated the use of transition probability geostatistics to aid in evaluating the continuity of zones expected to liquefy at different seismic loadings in the alluvial foundation of a proposed embankment dam. Krage (2018) further examined the impacts of conditioning the transition probability realizations to different levels of site investigations and concluded that a mean length to site investigation boring/sounding spacing ratio of at most 0.5 was required to reasonably constrain the soil category realizations. Munter et al. (2017) and Pretell et al. (2020) presented two-dimensional (2D) case histories on Cark Canal and the gently sloping Balboa Boulevard site, respectively, using conditional transition probability methods to better estimate seismic deformations experienced at each site. Those two studies demonstrated that realistic modeling of the relative proportions (i.e., sills) of the liquefiable and nonliquefiable soil types was necessary for obtaining agreement with seismic lateral spreading deformations observed in the field. Geostatistical methods for representing stratigraphic uncertainty may have significant limitations in approximating certain depositional environments (e.g., nonstationary properties, variably inclined bedding) or may be challenging to apply with insufficient exploration data, indicating the need for further development of these methods for geotechnical applications (e.g., Wang et al. 2018).

This case study presents an application of a Markov based conditional transition probability method for interpreting subsurface stratigraphy for the interbedded alluvium underlying Perris Dam and evaluating the effects stratigraphic uncertainty on NDA results for design earthquake loading. The purpose is to evaluate implementation challenges and potential benefits with Perris Dam chosen because the site characterization data constitutes a high standard of practice for quality and detail, and characterizing the spatial distribution of liquefiable lenses was a design concern. The challenges involved in synthesizing information from different sources (i.e., geologic conditions, different site investigation tools, lab data, field classifications) into soil categories for interbedded alluvium are examined. The application of conditional transition probability methods for developing three-dimensional (3D) realizations of the alluvial strata over a 305 m wide interval along the dam alignment is described including the challenges with insufficient data and limitations involved with utilizing a stationary, geostatistical method for approximating nonstationary geologic conditions. Five 2D cross sections for NDAs of Perris Dam are created by obtaining cross sections from 3D transition probability realizations. The PM4Sand and PM4Silt constitutive models were used to model the sand and clay soil categories in the alluvial strata, as well as the different zones in the embankment. The deformation magnitudes and variability for each cross section are compared and sensitivity studies are performed to examine the impact of several factors including the small strain shear modulus for the alluvium, mean lengths and sills for the alluvium categories, strengths for each alluvium soil category, and different ground motions. NDA cross sections of Perris Dam with uniformly (non-categorical) distributed properties are performed with and without additional deterministic imbedded soil lenses, and the deformations are compared with the transition probability models and deterministic models previously completed (URS 2012). The use of the conditional transition probability models for NDAs of Perris Dam, along with the implications and lessons for practice, are discussed.

Perris Dam

Perris Dam, located in Riverside County, California, is a compacted earthen embankment dam completed in 1973. The dam is approximately 3.5 km long, with two approximately equal-length reaches separated by a granitic outcrop near the dam's midpoint, as shown in Fig. 1. The dam reaches approximately 37 m tall with 1V:4H slopes upstream and 1V:3H slopes downstream. The dam consists of a clayey sand shell with a sandy clay core and is built on Holocene and late Pleistocene stream and slope wash deposits that consist primarily of silty sands and clayey sands with occasional lenses of poorly graded sand, well-graded sand, poorly graded gravel, sandy silt, and lean clay. The depth to weathered bedrock varies along the dam from 0 m deep near the abutments to 38 m deep over the central portion of the left reach. Since completion of the dam in 1973, an increased population downstream of the dam has warranted several engineering assessments and one major modification of the dam. The dam is located near several faults including the Elsinore and San Jacinto faults.

Several past studies have been completed to address the seismic risk of Perris Dam. The most recently completed study of Perris Dam, described in URS (2012) and compared further in Friesen et al. (2014), included three different NDA models completed by two different engineering groups with two different constitutive models. The first set of NDAs was completed by the URS engineering group using the UBCSAND constitutive model (Beaty and Byrne 2011) for the alluvial strata and it produced estimated crest settlements of 0.6-0.9 m for the design earthquake loading. The second set of NDAs was completed by the URS engineering group using the Pore Pressure Generation (PPG) constitutive model (Dawson et al. 2001) for the alluvial strata and it produced estimated crest settlements of 1.6 m. The third set of NDAs was completed by the California Department of Water Resources (DWR) engineering group using the Mohr-Coulomb constitutive model with residual strengths applied to liquefiable zones for the alluvial strata and it produced estimated crest settlements of 3.4 m. These deformations represent a wide range of deformations depending on the engineering group that performed the NDA and the choice of constitutive model in the alluvium. The results of these studies led to a major seismic retrofit completed in 2018 that included an additional berm and Cement Deep Soil Mixed (CDSM) walls constructed just downstream of the original downstream toe in an area where liquefiable lenses in the foundation were a concern. The analyses in this study focus on the pre-retrofit condition of Perris Dam without the recently installed CDSM walls or berm.

Geologic setting

Geologic context is important to aid in the assessment of soil categories, boundaries and properties. Perris Dam is located in an area of recently uplifted granitic rock called the Central Perris Block that has undergone several cycles of alluvial erosion and deposition since the end of the Miocene epoch. These cycles have weathered the granitic bedrock closer to the surface and has covered it in two strata of interbedded alluvium that underlie the dam as shown in the longitudinal profiles of the left reach of the dam in Fig. 2. The bedrock beneath the embankment was eroded by water flowing out of the Perris Block followed by a period of aggradation of interbedded alluvium leaving behind a deep notch in the weathered bedrock near station 99+20 (see Fig. 2) that widens out beneath the rest of the dam resulting in a deeper layer of alluvium in this area (Rennie et al. 2005). As the notch in the bedrock widens out towards the current ground surface the depositional environment of the alluvium also changes. Due to this change in depositional conditions and the different soil characteristics resulting from this change, the alluvium (previously designated as Qal by Rennie et al. 2005) is divided into a deeper Pleistocene Alluvium (designated as Qp) and a shallow Holocene Alluvium (designated as Qh) at a depth of approximately 6 m (URS 2012). Previously created NDA models have focused on station 99+20 which was the station with the greatest concerns for liquefaction and the largest expected deformations.

The present study focuses on the reach between stations 94+20 and 104+20 (red box in Fig. 2) for geostatistical modeling based on an evaluation of subsurface stratigraphic variations along the dam alignment. The reaches to the left or right of this central section have less Qp (i.e., shallower bedrock) and were judged to have notable differences in stratigraphic characteristics in the Qh. The 305 m (1000 ft) reach between stations 94+20 and 104+20 (stations numbers based on ft) has stratigraphic characteristics for both the Qp and Qh strata that appear relatively consistent with the assumption of stationarity, which is a required assumption for the geostatistical modeling method used. Separate geostatistical models would need to be developed for reaches to the left and right of this central section. The NDA models focus on station 99+20 with additional NDAs at stations 94+20, 96+70, 101+70, and 104+20, where the next closest rows of site investigation data are located (see Figs. 1 and 2 for locations of site exploration holes and soundings).

Site investigation data analysis for the alluvium

A thorough site investigation was completed in several stages along Perris Dam prior to the seismic retrofit as shown in Figs. 1 and 2. These investigations included borings with and without Standard Penetration Tests (SPTs) as well as Cone Penetration Tests (CPTs) with and without downhole seismic testing for shear wave velocity (V_s) profiling which will together be used to assess both soil categories and material properties. Between stations 94+20 and 104+20 a total of 19 borings located primarily on the downstream shell and 13 CPT soundings located primarily downstream of the dam are used for the analyses. Each data set was examined separately to assess their suitability for use in conditional transition probability realizations of the alluvial foundation material.

The site investigation data were used to identify appropriate soil categories within each alluvial stratum, as well as the spatial characteristics and properties for each soil category. Three categories were found to adequately distinguish between dominant soil types and engineering characteristics. For this study, the soil categories chosen are: (1) a clay category comprised primarily of clayey sands and silty clays with some clayey silts and sandy clays that may exhibit clay-like behavior, (2) a non-plastic nonliquefiable sand category, and (3) a non-plastic liquefiable sand category. These three categories are hereby referred to as the clay category, the nonliquefiable sand category, and the liquefiable sand category, respectively. All soil samples were consistent with one of the three selected soil categories and it is therefore considered to be unlikely that an additional category or anomaly (e.g., Tang and Halim 1988) could be present in large enough quantities to affect seismic deformations. The clay category is susceptible to yielding, but not liquefaction, and is modeled with the PM4Silt constitutive model (Boulanger and Ziotopoulou 2019), a critical state based model designed for use with plastic silts and clays. The nonliquefiable and liquefiable sand categories are both modeled with the PM4Sand version 3.1 constitutive model (Boulanger and Ziotopoulou 2017), a critical state based constitutive model designed for use with non-plastic silts and sands. The criteria that differentiate each soil category are explained in the following paragraphs.

Interpretations of the SPT, CPT, V_s, and laboratory test data using common engineering correlations produced some significant inconsistencies in the estimated proportions for candidate soil categories, and thus an effort was made to resolve the inconsistencies using reasonable adjustments to the correlations used. The goals of the site investigation data analysis are to: (1) obtain categorical data of the alluvial strata with adequate spatial coverage to be used with a transition probability methods, (2) obtain categories with consistent proportions between site investigation methods, and (3) assess the distribution of properties so that uniform properties can be assigned for each category.

A total of 441 SPTs are used for conditioning the soil properties of the alluvial strata. The clay category was separated from the nonliquefiable and liquefiable categories based on examination of several different liquefaction susceptibility criteria as summarized in Armstrong and Malvick (2016). The different criteria are based on fines contents (FC) cutoffs that can range from 0 to 50% and plasticity index (PI) cutoffs that can range from 0 to 12. The final criteria used in these analyses is with a FC cutoff of 35% and a PI cutoff of 7, which correspond to suggestions from Boulanger and Idriss (2006). Field classifications based on USCS classification (ASTM D2487-17e1) are used in the absence of laboratory classification data (i.e., FC, PI or USCS classification). Corrected blow counts, $(N_1)_{60cs}$, for the nonliquefiable and liquefiable sand categories are calculated with corrections from Boulanger and Idriss (2008) and an additional long-rod energy correction factor based on α=1%/m (i.e., reduction in delivered energy per meter of rod length) as applied to a similar embankment dam in Tatone et al. (2018). The cyclic resistance ratio ($CRR_{M=7.5}$) of the nonliquefiable and liquefiable sand categories are based on the $(N_1)_{60cs}$ with the Boulanger and Idriss (2012) liquefaction triggering correlation. Liquefiable sand was distinguished from non-liquefiable sand based on $CRR_{M=7.5} < 0.6$. The choice of liquefaction susceptibility criteria to differentiate the clay category from the sand categories and the $(N_1)_{60cs}$ cutoff to differentiate the nonliquefiable sand category from the liquefiable sand category significantly affected the proportions of each category and the strengths assigned to each category.

The soil category proportions were also evaluated using the thirteen CPT soundings between stations 94+20 and 104+20. The assumption that the soil category proportions obtained through CPTs are consistent with those obtained through SPTs requires a stationary condition across the site which may not be entirely correct. The value of the soil behavior type index (I_c) that separates clay-like from sand-like behavior is commonly taken as 2.6 (Robertson 2009). The value required to obtain the same proportions from the CPT data that were present in the SPT data is 2.45 for the Holocene Alluvium and 2.7 for the Pleistocene Alluvium, which seem to be reasonable adjustments for a site-specific application. Corrected cone tip resistances, q_{c1Ncs}, for the nonliquefiable sand and liquefiable sand categories are calculated with corrections from Boulanger and Idriss (2015). Fig. 3 shows a vertically exaggerated cross section of Perris Dam at station 99+20 with the site investigation data obtained from this station interpreted based on soil category. In this figure, an I_c value of 2.45 is used to separate the clay category from the sand categories in the Holocene Alluvium, an I_c value of 2.7 is used to separate the clay category from the sand categories in the Pleistocene Alluvium, and a $CRR_{M=7.5}$ value of 0.6 (based on the CPT correlation by Boulanger and Idriss 2015) is used to separate the nonliquefiable and liquefiable sand categories in both alluvial strata. This interpretation of the CPT data is reasonably consistent with, and supports, the interpretation based on the SPT and laboratory index test data.

Transition Probability Modeling for Alluvial Strata

The use of conditional transition probability (Carle and Fogg 1997) for stochastically representing the spatial variability of interbedded soils in NDAs of embankment dams holds the potential for more realistic predictions of the magnitude, uncertainty, and pattern of deformations due to their ability to better represent uncertainty in the stratigraphy between site investigation locations. Assigning soil properties for the Perris Dam alluvial strata in NDAs are complicated by the interbedded alluvium, prompting the assessment of transition probability methods to examine the impacts of stratigraphic uncertainty on the calculated deformations. Traditionally, the interbedded alluvium strata has either been simplified into representative soil groups and assigned representative properties (referred to as uniform models) or has been subdivided with additional lenses of uniform properties (referred to as uniform models with lenses) based on the judgement of the modelers (URS 2012). Transition probability is used in this study to create realizations based on the soil categories assessed from the site investigation data as a potential alternative to subjectively assigning alluvial subgroups/lenses.

Transition probabilities for three primary categories

Transition probability (Carle and Fogg 1997) is used to create realizations of the alluvial soils based on discretized soil categories (i.e., clay, nonliquefiable sand, and liquefiable sand categories) from site investigation data. Transition probability uses the soil category data to assess the probability of transitioning from one discrete soil category to another (e.g. from clay to nonliquefiable sand) based on the lag distances, in each orthogonal direction, between pairs of categorical data points. For example, if there are only two pairs of data at a horizontal lag distance of 10 m (within specified directional lag and angle tolerances), and the data pairs transition from clay to nonliquefiable sand and from clay to liquefiable sand, the probabilities of transitioning from clay to nonliquefiable sand or nonliquefiable sand to clay will be 0.5, from clay to liquefiable sand or from liquefiable sand to clay will be 0.5 and from any other category to any other category, including from one category to itself, will be 0 at that lag distance and in that direction. Data pairs are aggregated together to form transition probability data points when their lag spacing is within a user-specified lag tolerance (range of lag distances parallel to the direction of interest), bandwidth (range perpendicular to the direction of interest), and angle tolerance (angular range for considering the probability from one point to another) for a single orthogonal direction. The data points are then plotted in transiograms (graphs of transition probability plotted against lag distance) and used to fit 3D Markov chain models based on the overall proportions (referred to in geostatistical terms as sills) of each soil category and estimated mean lengths of each soil category so that soil realizations can be created. The sills and estimated mean lengths used for the Markov chain models in the baseline cases are presented in Table 1 and will be further explained in the following sections. The T-PROGS 7.0 software (Carle 1999) is used to create the 3D realizations of soil categories for the two Perris Dam alluvial strata for use in the NDA models. Further description of the required input properties for the T-PROGS model can be found in the T-PROGS 7.0 Manual (Carle 1999).

The vertical transiogram matrix is shown for the Holocene Alluvium baseline realizations in Fig. 4. The black dots represent the transition probabilities obtained from the SPT data at various lag distances, with a specified lag spacing of 0.5 m, lag tolerance of 0.25 m, bandwidth of 0.2 m, and angle tolerance of 22°. The black lines represent the Markov chain model used to represent transition probability for locations without direct knowledge of their soil category. The sills are directly input based on the proportions of each soil category present in the SPT data and the mean lengths were estimated based on the SPT data and a geologic interpretation of the depositional environment. Mean lengths are interpreted from a transiogram as the distance between a zero lag distance and the intersection point between an asymptotical line from the modeled line at the zero lag distance and an asymptotical line from the modeled line at an infinite lag distance (the sill) in the self-transition graphs (along the diagonal). An example of the mean length interpretation for the clay category is shown in red dashed lines in Fig. 4. This choice of mean lengths can therefore be subjective based on a fit to the data and will be examined as a source of uncertainty in further analyses. The baseline interpretation for the Holocene Alluvium, as shown in Fig. 4 and listed in Table 1, corresponds to sills of 46%, 28%, and 26% for the clay, nonliquefiable sand, and liquefiable sand categories, respectively, and vertical mean lengths of 1.0 m for all three categories. The sills for each category are the same in all directions for each alluvial strata.

The transiogram matrix in the along channel direction is shown for the Holocene Alluvium baseline realizations in Fig. 5. The largest distance between data points is approximately 110 m whereas the NDA models are 540 m long. This discrepancy in distances requires an assumption of stationarity in the transition probabilities for the size of the NDAs so that the transition probabilities assessed in locations where the data is present can be applied in locations where data is not present. This assumption may not be fully justified as seen by comparing the distributions of $(N_1)_{60cs}$ in Fig. 2 at different locations, however, it is a pragmatic simplifying assumption that is required in the absence of additional data. The existence of gradually changing depositional environments, and previously undetected geologic conditions or stratums may further reduce the applicability of the stationarity assumption to real geologic conditions. Fig. 5 also shows some data points plotting at 0 probability at longer distances (i.e, around 100 m, 140 m and 160 m) which are caused by the lack of data at those longer distances. This illustrates that data points based on a low number of data pairs are generally not reliable data points to fit the Markov chain model which can often occur at distances approaching the maximum distances of the site investigations. The baseline interpretation for the Holocene Alluvium, with the data shown in Fig. 5, a specified lag spacing of 20 m, a lag tolerance of 10 m, a bandwidth of 1 m, and an angle tolerance of 2°, corresponds to mean lengths in the along-channel direction of 25 m for all three categories (Table 1).

The transiogram matrix in the cross-channel direction is shown for the Holocene Alluvium baseline realizations in Fig. 6. This data direction only has five lag distances based on the five along-channel (upstream-downstream) rows of SPT data with a specified lag spacing of 20 m, a lag tolerance of 10 m, a bandwidth of 1 m, and an angle tolerance of 2°. The other data points on these graphs all have a zero transition probability because there are no pairs of data separated by those lag distances. Fig. 6 intentionally uses a low lag spacing in relation to the SPT spacing to illustrate the importance of lag spacing on the data points presented in transiograms. Lag distances that are too small will create zero probability data points that are the result of no data at that distance, but lag distances that are too large will group too many data pairs into single data points and will not provide enough resolution to fit the Markov chain models. The availability of sufficient data pairs for each data point can greatly impact the data points plotted in transiograms and therefore can impact the fit of the Markov chain models and the creation of the conditional soil category realizations. Careful selection of lag spacing, orthogonal direction angle (azimuth or dip), tolerances and bandwidths, with consideration of the geologic conditions, available site investigation data, ability to fit the data to a Markov chain model and application of the realizations (i.e., 2D NDAs) will impact the availability of data pairs for each data point and can therefore be an important step prior to interpreting the data for fitting the Markov chain models. While each of these parameters used for each point can be changed, it is important to make sure that each data point used to fit the Markov chain model is comprised of enough pairs of data so that the transition probability at that lag distance is stable (i.e., will not significantly change with the addition of more data pairs). The baseline interpretation for the Holocene Alluvium corresponds to mean lengths in the cross-channel direction of 10 m for all three categories (Table 1).

Conditional realizations for the alluvium

Seven 3D conditional transition probability realizations of each alluvial stratum were created and are used as the baseline realizations. Each of these seven realizations are conditioned on 441 SPT data points with the soil categories between the known locations assigned based on transition probability. The CPT data informed the geostatistical models as discussed previously, but were not used for conditioning the realizations because: (1) conversion of CPT data to equivalent SPT data, or vice versa, would involve an additional empirical conversion relationship, (2) the differences in vertical data spacing between the CPT and SPT would require subjective averaging or smoothing of the CPT data so that it could be applied to the same stochastic realization grid as the SPT data and (3) it provided an opportunity to compare the realizations conditioned on one set of data against the stratigraphy in the omitted data. Each realization is sliced into five cross sections as stations 94+20, 96+70, 99+20, 101+70 and 104+20 based on the locations of the rows of site investigations (see Figs. 1 and 2). The bottom of the Pleistocene Alluvium realizations are trimmed to contour the top of the weathered bedrock. The models generated at the five cross sections from one 3D realization are shown in Fig. 7. The models generated at station 99+20 from each of the seven different 3D realizations are shown in Fig. 8. The proportions and mean lengths for each soil category can be visually assessed from these realizations to confirm their consistency with the parameters listed in Table 1. For example, the dark blue zones (Pleistocene Alluvium liquefiable sand category) in Figs. 7 and 8 are visually consistent with the proportion (9%), vertical mean length (1.0 m) and along channel mean length (25 m) listed in Table 1 for this category and stratum.

NDA embankment models

This section describes the Perris Dam NDA configuration, material properties and constitutive model calibrations, stochastic and uniform model parameters, initialization of static stress conditions, and dynamic loading procedures. The Perris Dam NDAs are modeled and analyzed using the FLAC 8.0 finite difference program (Itasca 2016). The details of these modeling procedures and input parameters all have an influence on the deformations obtained in an NDA. Furthermore, the overall accuracy of any NDA modeling procedure is dependent on limitations inherent to continuum modeling, constitutive models, and numerical procedures. These limitations are, however, not expected to affect the relative influences of different stochastic realizations, given the same modeling procedures are used in all cases.

Embankment and foundation configurations

The embankment dam consists of the shells (same soil type in the upstream and downstream zones) and an upstream sloping clay core. A core trench was excavated during original construction to a depth of 3 m into the Holocene Alluvium, as shown on the cross sections in Figs. 7 and 8. The foundation is comprised of the 6 m thick Holocene Alluvium and the deeper Pleistocene Alluvium that varies in thickness from 21 m at STA 104+20 to 26 m at STA 99+20. The Holocene and Pleistocene strata are further discretized into the soil categories for the transition probability models as previously described. The Pleistocene Alluvium stratum is underlain by a 15 m thick weathered bedrock layer, which is in turn underlain by a 12 m thick bedrock layer. The reservoir level at the time of shaking is set to 4 m of freeboard which is consistent with previous analyses (URS 2012).

Material properties and constitutive model calibrations

The bedrock, weathered bedrock, shells and core materials use uniform material properties similar to those used in URS (2012). The bedrock is modeled as linear elastic with a Poisson's ratio of 0.3, a shear modulus of 16.9 GPa, and a saturated density, ρ, of 2.3 Mg/m^3, which correspond to a shear wave velocity, V_s, of 2700 m/s. The bedrock permeability is $1.8x10^{-4}$ cm/s. The weathered bedrock is modeled as linear elastic with a Poisson's ratio of 0.3, a shear modulus of 836 MPa, and a saturated density, ρ, of 2.3 Mg/m^3, which correspond to a shear wave velocity, V_s, of 600 m/s. The weathered bedrock permeability is $3.5x10^{-6}$ cm/s. The shells and core are modeled as a Mohr-Coulomb material with undrained shear strengths for the dynamic loading phase computed based on the initial static consolidation stresses using the procedures in Duncan and Wright (2005) as applied to NDA models by Montgomery et al. (2014). For the embankment shells, the undrained shear strength parameters for isotropic consolidation are d_R = 86 kPa and ψ_R = 13°, and the drained shear strength parameters are d_S (or c') = 0 and ψ_S (or ϕ') = 33°. The shear moduli for the shells are set proportional to the square root of the mean effective stress (p'), with G = 111 MPa at p' = 101.3 kPa. The permeability of the shells is $3.5x10^{-5}$ cm/s and the saturated density is 2.2 Mg/m^3. For the core, the undrained shear strength parameters for isotropic consolidation are d_R = 62 kPa and ψ_R = 14.5°, and the drained shear strength parameters are d_S (or c') = 0 and ψ_S (or ϕ') = 22°. The shear modulus for the core is set proportional to the square root of the mean effective stress (p'), with G = 95 MPa at p' = 101.3 kPa. The core permeability is $3.5x10^{-6}$ cm/s and the saturated density is 2.1 Mg/m^3.

The constitutive models and material properties for the soil categories in the Holocene (Qh) and Pleistocene (Qp) alluvial strata are presented in Table 2. The 30th percentile $(N_1)_{60cs}$ values from the liquefiable and nonliquefiable categories are used to select uniform input parameters for the PM4Sand constitutive model. The contraction rate parameter (h_{po}) for the sand-like materials is calibrated based on single-element direct simple shear simulations to match the cyclic resistance ratio ($CRR_{M=7.5}$) based on the SPT based liquefaction triggering correlation from Boulanger and Idriss (2012). The $CRR_{M=7.5}$

was limited to 0.6 for the nonliquefiable sand category to prevent this category from being overly strong. A normalized undrained shear strength ratio, $S_{u,ce,eq}/\sigma'_{vc}$, value of 0.3 is used for the clay category with the PM4Silt constitutive model based on monotonic and cyclic direct simple shear tests of tube samples (Dahl 2011). The contraction rate parameter (h_{po}) for the clay category is calibrated based on single-element direct simple shear simulations to match the $CRR_{M=7.5}$ estimated based on the above normalized undrained shear strength (Idriss and Boulanger 2008). The shear modulus coefficient (G_o) for all soil categories is calculated from the normalized shear wave velocity of 380 m/s at one atmosphere of overburden stress based on the data in Rennie et al. (2005).

Initial static stress conditions

Static stress and steady seepage conditions were initialized by simulating placement of the embankment in multiple lifts, followed by raising the reservoir level in a sequence of stages. The embankment and alluvial materials were modeled as Mohr-Coulomb materials with confinement-dependent moduli for these initial static analyses. The resulting distributions of pore water pressure, vertical effective stress, coefficient of lateral earth pressure at rest (K_o), and initial static shear stress ratio (α) were smoothly varying with distributions that were reasonable. The embankment and alluvial materials were then updated with their respective material models prior to dynamic loading.

Dynamic loading

Embankment dam models were subjected to six spectrally-matched bedrock outcrop input motions developed by URS (2009) based on a probabilistic seismic hazard analysis. The seed motions included three strong ground motion recordings and three synthetic time histories. The acceleration time series and their linear-elastic acceleration response spectra are shown in Fig. 9. The Arias Intensity (I_A) for these motions, as listed on Fig. 9, range from 3.5 m/s to 5.1 m/s. The input motion based on a 1978 M_w=7.4 Tabas earthquake recording was selected as the primary motion in analyses by URS (2012), and thus detailed parametric results are presented herein for this motion as well. Outcrop motions were applied as a shear stress time series to the compliant base of the embankment models (Mejia and Dawson 2006). Free field conditions were applied at the lateral edges of the models, with the outer column of elements on each edge of the alluvium replaced with an equivalent elastic material to improve lateral confinement on the soil columns. All materials were assigned Rayleigh damping of 0.5% at a frequency of 3 Hz to provide a minimum level of damping in the small strain range for the nonlinear materials and a nominal damping for the linear elastic bedrock material.

NDA results

The NDA results are summarized herein in terms of embankment deformations because they are often of primary concern for evaluating damages, while recognizing other aspects of the dynamic response can be equally important for evaluating the performance of a specific facility and need to be closely examined during quality control of any dynamic response study. Embankment deformations are obtained at the end of strong shaking for each of the five different cross sections with seven different realizations of the Holocene and Pleistocene Alluvium. Detailed parametric results are first presented for the Tabas input motion, with results for all six input motions presented later.

Embankment crest settlements (Δ_{set}) are obtained as the vertical deformation at the midpoint of the embankment crest. Embankment stretches (Δ_{str}) are the increase in embankment base length calculated as the difference in the outward horizontal displacements of the embankment toes. Embankment stretch is preferred over using the displacements of the two toes separately, because stochastic realizations sometimes result in a large outward displacement at one toe or the other, and the statistics on embankment stretch (which reflects large displacements at either toe) are better behaved than the statistics for displacement at either toe alone. Crest settlements are normalized by the original embankment height (H = 37 m) and embankment stretches are normalized by the original embankment base length (B = 267 m). Other measures of dynamic response can be important in certain situations, but embankment displacements are generally a primary concern in seismic evaluations. Comparisons of deformation uncertainty are evaluated by comparing sample standard deviations of the natural log of the normalized deformations for the set of realizations of each model, with the standard deviations computed based on Johnson and Bhattacharyya (2010) given the small number of cases examined.

Baseline cases

The normalized crest settlements and embankment stretches along with the standard deviation in the normal logarithm of the normalized settlements and stretches are presented in Fig. 10 for each cross section. The normalized settlements for the five cross sections range between 1.2% and 2.3% with the standard deviation in the lognormal of the normalized settlements ($\sigma_{ln(set)}$) ranging between 0.1 and 0.2. These settlements are similar in magnitude and variability across the five stations; STA 99+20 has a smaller variability than the other stations, but this may be attributable to the small number of realizations being used for each cross section alone. The normalized stretches range between 0.5% and 1.0% with the standard deviation in the lognormal of the normalized stretches ($\sigma_{ln(str)}$) ranging between 0.06 and 0.17. When deformations from all stations are grouped together, the $\sigma_{ln(set)}$ is 0.17 and the $\sigma_{ln(str)}$ is 0.15 as indicated with the orange dashed line in Fig. 10.

The impact of small strain shear modulus (G_{max}) in the alluvium

Sensitivity of the NDA results to the small-strain shear moduli (G_{max}) in the alluvium was evaluated by performing a set of analyses wherein the G_{max} for the alluvial strata are based on empirical correlations to the SPT data, rather than on the available V_s data. The V_s data from Rennie et al. (2005) correspond to G_{max} values that are 3.1 times greater than those obtained from the empirical correlation to SPT $(N_1)_{60cs}$ values by Andrus and Stokoe (2000), with the differences attributed to the effects of ageing and light cementation in these strata. For these models, the shear modulus coefficient was instead estimated based on the suggested correlation to SPT $(N_1)_{60cs}$ values in Boulanger and Ziotopoulou (2017), which is derived from the correlation by Andrus and Stokoe (2000). The shear modulus coefficient of the clay category was set to match the shear modulus coefficient of the nonliquefiable sand category. The contraction rate parameter was then adjusted based on the previously described calibration procedure with the new shear modulus coefficient.

The normalized deformations and their standard deviations are presented in Fig. 11 for the models calibrated with the smaller small-strain shear moduli in the alluvium. The normalized settlements range between 1.6% and 3.0% with $\sigma_{ln(set)}$ ranging between 0.11 and 0.18. The normalized stretches range between 0.9% and 1.5% with $\sigma_{ln(str)}$ ranging between 0.05 and 0.1. The deformations are generally similar between each station. The $\sigma_{ln(set)}$ values are larger than the $\sigma_{ln(str)}$ values indicating a smaller variability in normalized stretches. The revised calibration results in an approximately 30% increase of both crest settlements and embankment stretches, while the peak horizontal acceleration at the crest decreased by about 11%. The response spectra for the crest motion indicates the fundamental period of the dam increased by about 5% from 0.4 seconds to 0.42 seconds. These results are attributed to greater strains developing in the alluvium despite a slight reduction in the imposed dynamic shear stresses.

The impact of alluvial mean lengths

A set of analyses was completed with the mean lengths of all three soil categories in the alluvial strata (Table 1) doubled. The doubled mean lengths provide an upper-range (larger) estimate of mean lengths while maintaining reasonable fits to the transition probability data (Figs. 4-6). All other soil parameters and calibrations remained the same as the baseline cases.

The normalized deformations and their standard deviations are presented in Fig. 12 for each cross section with the alluvial mean lengths doubled from the baseline cases. The normalized settlements range between 1.2% and 2.4% with $\sigma_{\ln(set)}$ ranging between 0.12 and 0.19. The normalized stretches range between 0.4% and 1.1% with $\sigma_{\ln(str)}$ ranging between 0.08 and 0.25. Deformations are generally similar between each station. When compared to the baseline cases presented in Fig. 10, the deformations and standard deviations of deformations are within similar ranges. Therefore, the mean lengths in both alluvial strata do not make a significant difference for these models.

The impact of varying the sill and mean lengths in the Pleistocene Alluvium

A set of analyses were completed with the Pleistocene Alluvium soil category sills and mean lengths set to the same values as the Holocene Alluvium. This was done to simulate a case where the boundaries between the Holocene and Pleistocene Alluvium was not set, but a slight increase in $(N_1)_{60cs}$ with depth is still acknowledged. This assumption increases the liquefiable sand sill in the Pleistocene Alluvium from 9.2% to 26.3% providing for an increased potential for a deeper deformation mechanism to develop in liquefiable sand lenses.

The normalized deformations and their standard deviations are presented in Fig. 13 for each cross section with the Holocene Alluvium soil category sills and mean lengths (Table 1) used for the Pleistocene Alluvium. The normalized settlements range between 1.4% and 2.4% with $\sigma_{\ln(set)}$ ranging between 0.10 and 0.17. The normalized stretches range between 0.6% and 1.0% with $\sigma_{\ln(str)}$ ranging between 0.06 and 0.14. Deformations are generally similar between each station and are only slightly greater than the deformations obtained in the baseline cases shown in Fig. 10. These results indicate that the embankment model is relatively insensitive to changes in the mean lengths and sills in the Pleistocene Alluvium which may be partially due to the greater strengths for the sand categories in the Pleistocene Alluvium preventing significant strains from developing in this deeper stratum.

The impact of different ground motions

A set of analyses was completed for the model at station 99+20 with the full set of six spectrally matched input motions (Fig. 9). An additional set of analyses was completed for the model at station 99+20 with the Tabas motion scaled by a factor of 1.5 to a PGA of 0.6 g (hereby referred to as Tabas x 1.5), giving the scaled motion an I_A of 8.2 m/s. This motion is used to represent a loading scenario with a greater PGA than the motions obtained from Wong et al. (2009) and used in URS (2012).

The normalized deformations and their standard deviations are presented in Fig. 14 for the station 99+20 baseline models subjected to the six spectrally matched motions and the Tabas x 1.5 motion. The normalized settlements for the spectrally matched motions (i.e., all motions except for the Tabas x 1.5 motion) range between 1.0% and 2.4% with $\sigma_{ln(set)}$ ranging between 0.09 and 0.10. The $\sigma_{ln(set)}$ values are similar between all motions. The normalized stretches for the spectrally matched motions range between 0.5% and 1.1% with $\sigma_{ln(str)}$ ranging between 0.05 and 0.1. When the deformations using the spectrally matched motions are grouped together, the $\sigma_{ln(set)}$ is 0.24 and the $\sigma_{ln(str)}$ is 0.23 as indicated by the orange dashed lines in Figs. 14c and 14d. Comparing the $\sigma_{ln(set)}$ and $\sigma_{ln(str)}$ for all stations (approximately representing the variability resulting from different realizations) in Fig. 10 to the $\sigma_{ln(set)}$ and $\sigma_{ln(str)}$ for spectrally matched motions (approximately representing the variability resulting from different realizations and different spectrally matched motions) in Fig. 14, the results indicate that the variability in embankment deformations for this set of motions and realizations include approximately equal contributions from the ground motions and alluvial variability. I_A has been observed to be one of the more effective intensity measures for estimating crest settlements of embankment dam (e.g., Armstrong et al. 2018), where the embankment crest settlements increase with increasing I_A. The analysis sets for each ground motion are ordered in Fig. 14 with the first 3 columns based on recorded seed motions in the order of their I_A values and the second 3 columns based on synthetic seed motions also in order of their I_A values. The deformations were similar for either set of seed motions and generally increased with increasing I_A.

The Tabas x 1.5 motion increased the median normalized settlement by about 35% and increased the normalized stretch by about 40% relative to those for the base Tabas motion. The $\sigma_{ln(set)}$ and $\sigma_{ln(str)}$ for the Tabas x 1.5 motion both decreased by approximately 0.01 when compared to models that were subjected to the base Tabas motion. These modest increases in deformations, given a 50% increase in the base motion along with the slight decreases in the variability of deformations, indicate that the embankment is not brittle to increased seismic loadings. When comparing the deformations to the other spectrally matched motions, the general trend of increasing deformations with increasing I_A but minimal change in variability with I_A is observed.

The impact of different soil category strengths

A set of analyses was completed for the model at STA 99+20 with a range of different $(N_1)_{60cs}$ used in the liquefiable sand category and a range of different $S_{u,cs,eq}/\sigma'_{vc}$ used in the clay category in both the Holocene and Pleistocene Alluviums. The $(N_1)_{60cs}$ used in the liquefiable sand category was reduced to 50% (the red triangles) and 25% (the green triangles) of the $(N_1)_{60cs}$ used in the liquefiable sand category baseline cases (the blue triangles). These values represent possible conservative soil properties (less than the 30^{th} percentile from site investigation data) in the liquefiable sand category. The $S_{u,cs,eq}/\sigma'_{vc}$ used in the clay category was changed to 0.2 and 0.4 representing a possibly more conservative case and possibly less conservative case (closer to mean strengths from direct simple shear tests from Dahl 2011). The nonliquefiable sand category remains unaltered for all cases.

The normalized deformations and their standard deviations are presented in Fig. 15 for each cross section with different soil category properties in the alluvium. The crest settlements for these cases range from 1.3% to 5.8% and the embankment stretches range from 0.6% to 2% with the largest deformations resulting from cases with the lowest liquefiable sand blow counts and lowest clay strength. The deformation standard deviations generally remain within the range of 0.11 to 0.34 for crest settlements and within the range of 0.06 and 0.23 for embankment stretches with larger values corresponding to stations with one or two models producing much larger deformations. This indicates that even small liquefiable lenses (representing 26.3% of the material in the Holocene Alluvium and 9.2% in the Pleistocene Alluvium) can produce much larger deformations if their strengths are very low. These outlier cases occur primarily when strains in the alluvium below the downstream shell concentrate in a few liquefiable zones due to the weaker properties of those zones or the geometry of stronger zones around them.

Uniform models

A set of models was completed for all stations subjected to the Tabas motion with the Holocene and Pleistocene Alluvium each represented by a single soil category. For example, if the Pleistocene Alluvium is represented by nonliquefiable sand, three different models are created with the Holocene Alluvium represented by clay, nonliquefiable sand, and liquefiable sand categories. Models with liquefiable sand used for the Pleistocene Alluvium are not performed due to the low proportion of liquefiable sand (9.2%) found in this stratum.

The normalized deformations and their standard deviations are presented in Fig. 16 for the STA 99+20 models with different combinations of uniform soil groups in the Holocene and Pleistocene Alluvium. The normalized settlements range between 1.1% and 3.0%. The normalized stretches range between 0.3% and 1.4%. These small ranges of deformations along with the small strains that propagate through the embankment indicate that the embankment is generally strong enough to prevent significantly larger deformations, however, there are still a few trends that can be observed from the uniform models. The models with the clay category in the Pleistocene Alluvium produce greater deformations than models with the nonliquefiable sand category in the Pleistocene Alluvium. The models with the liquefiable sand category or the clay category in the Holocene Alluvium produced greater deformations than models with the nonliquefiable sand category in the Holocene Alluvium. These trends indicate that the category that deforms the least is the nonliquefiable sand, followed by the clay, and then the liquefiable sand. However, the Qh clay, Qp clay models tend to produce greater deformations than the Qh liquefiable sand, Qp nonliquefiable sand models which may be primarily due to the same $S_{u,ce,eq}/\sigma'_{vc}$ value used in both layers for the Qh clay, Qp clay models as opposed to the differences in $(N_1)_{60cs}$ (Qh $(N_1)_{60cs}$= 14 and Qp $(N_1)_{60cs}$= 39) used in the Qh liquefiable sand, Qp nonliquefiable sand models. Using the same strength between the strata allow the shear strains in the Qh clay, Qp clay models to propagate in both a horizontal band along the Holocene Alluvium and a downstream circular deformation mechanism that extend into the Pleistocene Alluvium, whereas using a greater difference in strength from different $(N_1)_{60cs}$ values used for each stratum in the Qh liquefiable sand, Qp nonliquefiable sand models results in concentration of the shear strains along the Holocene Alluvium. Fig. 16 also indicates a greater difference in deformations as a result of the assumed category used in each alluvial stratum than from each station, indicating that the soil category used in each stratum is of greater importance to the estimated deformations than the geometric differences from each station. Collectively. the uniform models produce a greater range of deformations than the baseline models and all of the other sensitivity studies that use the same strengths. This indicates that using uniform models with different controlling soil categories in the alluvium strata would, for these models, provide bounds on the range of potential deformations.

Uniform models with deterministic imbedded lenses

A set of analyses were performed using a stratigraphic model based on engineering judgment rather than geostatistical realizations, similar to what was done in previous engineering studies for this dam. Fig. 17 shows (a) the URS (2012) model with deterministic embedded lenses in various locations and (b) the recreated model used in this study. These models are similar with the few exceptions being the inclusion of the core trench and the exclusion of the Zone 3/4 in the recreated model. The properties of Zone 3/4 were generally consistent with the shell (Zone 2 in Fig. 17(a)) with the exception of a higher friction angle and therefore the exclusion of this zone may be slightly conservative. The recreated model was analyzed with four different calibration assumptions based on whether the G_{max} values were based on V_s data or the empirical correlation to $(N_1)_{60cs}$ (as was completed for transition probability models in the previous section) and whether the $(N_1)_{60cs}$ values used were consistent with those used in URS (2012) or were decreased by 10%. The normalized crest settlements are between 1.3% and 2% and the normalized stretches are between 0.3% and 0.5%, which are similar to the deformations obtained with the baseline models (Fig. 10) and are slightly less than the deformations obtained by URS using the UBCSAND model (URS 2012). The range of deformations is within the range of deformations obtained with the uniform models indicating that while the inclusion of interpreted lenses may be important in other NDAs, in this case, it did not have a significant effect on the estimated deformations. These results also suggest that the use of deterministic lenses in interbedded deposits can be a reasonable approach in practice for evaluating their potential significance, before undergoing the effort to represent soil variability with stochastic methods. Therefore, using different controlling uniform soil categories provides a larger range of deformations from which the potential deformations can be bounded.

Post-shaking residual strengths

Post-Shaking analyses were completed for each of the baseline cases and for those sensitivity studies involving lower shear strengths, different motions, and different mean lengths and sills. For these cases, elements were assigned a case-history based residual strength at the end of shaking if their maximum shear strains exceeded 3% or their excess pore pressure ratios (r_u) exceeded 70% at any time during shaking. Residual strengths were calculated based on the strength ratio approach with potential void redistribution effects in Idriss and Boulanger (2015). The post-shaking analysis continued in time until the system reached a new static equilibrium. Deformations at the end of these post-shaking analyses were all less than 1% greater than those at the end of strong shaking, indicating that all the models were stable after shaking. These results indicate that even when very low residual strengths were assigned to liquefiable sand lenses in the Holocene and Pleistocene Alluvium, the strengths of the other soil categories and overlying embankment were sufficient to maintain stability.

Discussion

Synthesis of soil data from a variety of site investigation sources (i.e., interpreted geology, CPT, SPT, shear wave velocity, etc.) into a single consistent database to use in transition probability methods is complicated by several different factors. Geologic conditions may cause difficulties in the synthesis of data induced by geologic boundaries that are not well constrained, non-stationarity of soil properties, and juxtaposition of soil layering. These geologic conditions are often the result of complex depositional processes that vary both spatially and temporally. The simplifying assumptions inherent to many geostatistical modeling methods, such as stationarity, can often be difficult to validate, especially with limited data, and may significantly impact estimated deformations. Interpretation of soil characteristics can be challenging when considering intermediate and interbedded soils, especially when those soils may be affected by physiochemical processes such as cementation and aging. Correlations from site investigation data to factors used in NDAs also have variability and are often based primarily on data for clean and uniform soils. Each of these factors can impact the soil behavior category designations, sills, and mean lengths used in the transiograms that determine the spatial distribution of properties in subsurface realizations.

Once a database of soil behavior types is synthesized from the site investigation data, the creation of subsurface realizations from transiograms of soil behavior types is further complicated when insufficient data makes defining transiograms subjective to interpret and model. Insufficient data may result from soil categories that comprise a low proportion (a low sill) of the overall material, as is the case with liquefiable sand category in the Pleistocene Alluvium stratum. Due to practical site investigation considerations (vertical drilling, use of grid patterns for site investigations, etc.) it is common for there to be adequate data in the vertical direction, but not in both horizontal directions or across the full footprint of an embankment (especially on the upstream side for operating reservoirs). Common practice of using equally spaced grids also reduces the number of lag distances between transiogram data points providing the modeler with fewer points from which to model and adjust a transiogram (Krage 2018). The choice of mean lengths and therefore the shape of transiogram curves is often estimated based on a subjective fit of a model to often insufficient data.

A summary of the range of crest settlements for all Perris Dam analysis sets is shown in Fig. 18. The top three rows show the range of crest settlements obtained in prior studies for this dam. Analyses by URS produced crest settlements of 0.6 m to 0.9 m (Δ_{set}/H= 1.6-2.4%) using the UBCSAND model and about 1.6 m (Δ_{set}/H= 4.3%) using the PPG model, whereas analyses by DWR produced about 3.4 m (Δ_{set}/H= 9.2%) using the Mohr-Coulomb model (URS 2012). The large difference in crest settlements obtained by URS and DWR with the different constitutive models illustrate how details of the numerical modeling procedures (e.g., choice of constitutive model, calibration protocol, initialization of stresses, solution techniques) can greatly impact NDA results, and that resolving such differences requires a high level of documentation and quality control practices. The differences between these cases and the other cases summarized in Fig. 18 can be partially attributed to modeling procedures, differences in each set of cases, and programming differences from each modeling group, but are also partially attributed to some changes that have occurred since that time in the processing of soil data (e.g., addition of the long-boring correction, more widely accepted liquefaction susceptibility criteria, etc.), input of soil parameters (e.g., the use of anisotropically consolidated undrained strengths in the core) and updates to computer modeling (i.e, the use of FLAC 8.0 as opposed to previous versions).

The other cases summarized in Fig. 18 pertain to the parametric studies presented herein. NDAs completed with the use of transition probability in this study are generally consistent with the deformations obtained by URS with the UBCSAND model including the baseline cases, cases with the mean lengths doubled, models where the Holocene Alluvium transiograms were used in the Pleistocene Alluvium, and models using the other outcrop input motions. The largest range of crest settlements was produced by models that used different property assumptions for the liquefiable sand and clay categories. The larger deformations obtained with these models were obtained using properties that are considered to be over conservative. The two sets of uniform models (with and without imbedded lenses) were also in general agreement with the ranges obtained with the stochastic models herein or by URS using the UBCSAND model. The uniform models without lenses but with conservative category scenarios provided conservative bounds on the deformations. The uniform models with deterministic lenses were within the range of the baseline stochastic cases, but underestimated the full range that the stochastic realizations produced. The results of these comparisons suggest that uncertainty in the embankment deformations for Perris Dam included roughly equal contributions from uncertainties in the spatial variability of the alluvial strata, the properties assigned to the alluvial soils, and the input ground motions. The use of conditional transition probability as a means for generating foundation realizations did not have a dominant effect on the NDA results for this dam, but the process provided insights on merging data from geologic and geotechnical models as well as fostering improved communications across disciplines.

Shear strains for a baseline case, a case with double mean lengths and a uniform model with lenses is shown in Fig. 19. While the shear strains are different for each model, the primary mechanisms are generally similar. These primary mechanisms consist of: (1) a horizontal deformation mechanism beneath the downstream shell, but not intersecting the embankment, (2) a downstream circular deformation mechanism, and (3) an upstream circular mechanism with smaller shear strains than (1) and (2). These mechanisms are less evident in the uniform model with lenses due to the more uniform distribution of shear strains in the Qh stratum beneath the embankment. In all cases, maximum shear strains within the embankment do not exceed 6%, with the maximum shear strains in the alluvial stratum ranging from 8% to 24% depending on the model. These results indicate that for this particular embankment, the geometry and strength of the embankment strongly influence the deformation mechanisms which may decrease the impacts of the other influencing factors studied herein.

Conclusions

This case study presented an application of a Markov based conditional transition probability method for guiding interpretation of subsurface stratigraphy for the interbedded alluvium underlying Perris Dam and evaluating the effects of stratigraphic uncertainty on the NDA results for design earthquake loading. The challenges involved in synthesizing information from different sources (i.e., geologic conditions, different site investigation tools, lab data, field classifications) into soil categories for the two interbedded alluvial strata were examined. The application of conditional transition probability methods for developing 3D realizations of the alluvial strata over a 305 m wide interval along the dam alignment were described including the challenges with insufficient data and nonstationary geologic conditions. Two-dimensional NDA models were created by slicing seven different 3D transition probability realizations at five 2D cross sections each. The deformations and variability in deformations for each cross section were compared and sensitivity studies used to examine the impact of the small strain shear moduli for the alluvium, the mean lengths and sills for each alluvial category, the strengths for each alluvial category, and different ground motions. NDA cross sections of Perris Dam with uniform (non-categorical) properties, with and without deterministic embedded soil lenses were also analyzed. The full set of NDA results were further compared to results obtained by others in prior studies (URS 2012).

Deformations of Perris Dam obtained with NDAs that use transition probability are influenced by the entire analysis process including planning and conducting site investigations, synthesis and analysis of site investigation data into geologic models and soil categories, creation and interpretation of transiogram models and the culmination of these processes with the selection and calibration of soil properties. The planning of site investigations can impact the results of NDAs using transition probability if the spatial coverage and spacing between data are insufficient to adequately constrain the transition probability models. The synthesis and interpretation of the site investigation data into geologic models can be complicated due to the different limitations and correlations used with each site investigation method (e.g. CPT, SPT, Vs, lab, and field classification data). Even with substantial site investigation data, geologic transitions are often difficult to assess due to nonstationary or gradually transitioning properties. The creation and interpretation of transiogram models can be impacted by choice of lag spacing, orthogonal direction angle (azimuth or dip), bandwidths, tolerances and choices that impact the fit (e.g. soil category mean lengths and sills) of the Markov chain model to the data. The selection and calibration of soil properties can impact the overall deformations obtained in the NDAs as shown when comparing the deformations obtained through the baseline cases and cases with the G_{max} calibrated to $(N_1)_{60cs}$ and cases with different soil category strengths. While some of these sources of uncertainty have been shown to not significantly impact the overall deformations on their own, with each step of this process involving some level of subjectivity, the amalgamation of all of these sources of uncertainty may have significant impacts on the deformations. Due to these impacts, in combination with the complexity involved with transition probability and the programming involved in creating NDAs of embankment dams, a concerted quality control effort is required to ensure that the NDA models are working as intended.

In the case of the Perris Dam NDAs, the sources of uncertainty examined included various engineering and geostatistical properties for the different soil categories in the Holocene and Pleistocene alluvial strata (i.e., G_{max}, mean lengths, sills, strengths), the input motions, and the use of uniform models with and without deterministic imbedded soil lenses. The largest discrepancy in deformations for the transition probability models occurs with different soil category strengths (even though those properties may be overly conservative). The uniform models without lenses but with conservative category scenarios provided conservative bounds on the deformations. The uniform models with deterministic embedded lenses provided deformations within the range of the baseline stochastic cases, but underestimated the full range that the stochastic realizations produced. The results of these comparisons suggest that variability in the embankment deformations for Perris Dam included roughly equal contributions from variabilities in the spatial variability of the alluvial strata, the properties assigned to the alluvial soils, and the input ground motions. The use of conditional transition probability as a means for generating foundation realizations did not have a dominant effect on the NDA results for this dam, but the process provided insights on merging data from geologic and geotechnical models as well as fostering improved communications across disciplines.

The use of transition probability tools in NDAs has the potential to provide better estimations of deformations and deformation patterns than uniform model NDAs for cases where the assumptions of the geostatistical method (e.g., stationarity) are reasonably justified and the geostatistical parameters are reasonably constrained by site characterization data. This may be of value for geotechnical systems where uncertainties in the soil properties or ground motions are different than the case presented herein. Therefore, further development and evaluation of these procedures on other cases histories is warranted.

Data Availability Statement

Data that support the findings of this study available from the corresponding author upon reasonable request.

Acknowledgements

The work described herein progressed under projects for the California Department of Water Resources under Contract 4600009751 and the National Science Foundation under grant CMMI-1635398. Any opinions, findings, conclusions, or recommendations expressed herein are those of the authors and do not necessarily represent the views of these organizations. Professor Graham E. Fogg provided assistance with the transition probability modeling. Michael W. Driller and Steven Neumayr from the California Department of Water Resources provided useful insights that strengthened this paper. The authors appreciate the above for their support and assistance.

References

Andrus, R. D., and Stokoe, K. H. (2000). "Liquefaction resistance of soils from shear-wave velocity." Journal of Geotechnical and Geoenvironmental Eng., ASCE 126(11), 1015–025.

Armstrong, R. J., and Malvick, E. J. (2016). “Practical considerations in the use of liquefaction susceptibility criteria.” Earthquake Spectra, EERI, EERI. 32(3).

Armstrong, R. J., Kishida, T., and Park, D. (2020). “Efficiency of ground motion intensity measures with earthquake-induced earth dam deformations.” Earthquake Spectra, EERI, EERI. 21(1).

ASTM D2487-17e1, Standard Practice for Classification of Soils for Engineering Purposes (Unified Soil Classification System), ASTM International, West Conshohocken, PA, 2017.

Beaty, M. H., and Byrne, P. M., (2011). “UBCSAND Constitutive Model Version 904aR Documentation Report: UBCSAND Constitutive Model on Itasca UDM Web Site.”

Boulanger, R. W., and Idriss, I. M. (2006). “Liquefaction susceptibility criteria for silts and clays.” Journal of Geotechnical and Geoenvironmental Engineering, ASCE, 132(11), 1413-1426.

Boulanger, R. W., and Idriss, I. M. (2012). “Probabilistic SPT-based liquefaction triggering procedure.” Journal of Geotechnical and Geoenvironmental Engineering, ASCE, 138(10), 1185-1195.

Boulanger, R. W., and Montgomery, J. (2016). “Nonlinear deformation analyses of an embankment dam on a spatially variable liquefiable deposit.” Soil Dynamics and Earthquake Engineering, 91, 222–233.

Boulanger, R. W., and Ziotopoulou, K. (2019). "A constitutive model for clays and plastic silts in plane-strain earthquake engineering applications." Soil Dynamics and Earthquake Engineering, 127(2019): 105832, 10.1016/j.soildyn.2019.105832.

Boulanger, R. W., and Ziotopoulou, K. (2017). “PM4Sand (Version 3.1): A sand plasticity model for earthquake engineering applications”, rep. No. UCD/CGM-17/01, Center for Geotechnical Modeling, Dept. of Civil and Environmental Engineering, Univ. of California, Davis, CA.

Carle, S. F. (1999). T-PROGS: Transition probability geostatistical software. Davis, CA: University of California, Davis.

Carle, S. F., and Fogg, G. E. (1997). "Modeling Spatial Variability with One and Multidimensional Continuous-Lag Markov Chains." Mathematical Geology 29, 891–918 (1997). https://doi.org/10.1023/A:1022303706942

Dahl, K. R. (2011). "Evaluation of Seismic Behavior of Intermediate and Fine-Grained Soils." Ph.D. thesis, Davis, CA: University of California Davis.

Dawson, E. M., Roth, W. H., Nesarajah, S., Bureau, G., and Davis, C. A., (2001). "A Practice-Oriented Pore Pressure Generation Model." In Proceedings, 2nd FLAC Sumposium on Numerical Modeling in Geomechanics, Oct 29-31, Lyon, France.

Duncan, J. M., and Wright, S. G. (2005). Soil strength and slope stability. J. Wiley & Sons, Hoboken.

Friesen, S., Balakrishnan, A., Driller, M., Beaty, M., Arulnathan, R., Newman, E., and Murugaiah, S. (2014). "Lessons Learned from FLAC Analyses of Seismic Remediation of Perris Dam." Proc., 34th USSD Annual Meeting and Conference, United States Society on Dams, San Francisco, CA, April 7-11, 2014.

Idriss, I. M., and Boulanger, R. W. (2008). Soil liquefaction during earthquakes. Monograph MNO-12, Earthquake Engineering Research Institute, Oakland, CA.

Idriss, I, M., and Boulanger, R. W. (2015). "2nd Ishihara Lecture: SPT- and CPT-based relationships for the residual shear strength of liquefied soils." Soil Dynamics and Earthquake Engineering, ASCE, 2015, 68, 57-68.

Itasca (2016). Fast Lagrangian Analysis of Continua (FLAC), release 8.0. Itasca Consulting Group, Inc., Minneapolis, MN.

Joint TC205/TC304 Working Group (2017). "Discussion of statistical/reliability methods for Eurocodes – Final Report." 5th International Symposium on Geotechnical Safety and Risk, International Society for Soil Mechanics and Geotechnical Engineering, Rotterdam, Netherlands, 2015.

Krage, C. P., DeJong, J. T., and Boulanger, R. W. (2016). "Identification of geologic depositional variations using CPT-based conditional probability mapping."

Proceedings, 5th International Conference on Geotechnical and Geophysical Site Characterization, Gold Coast, Australia, September 5-9.

Krage, C. P. (2018). “Investigation of Sample Quality and Spatial Variability for Intermediate Soils.” Ph.D. thesis, Davis, CA: University of California Davis.

Langousis, A., Kaleris, V., Kokosi, A., and Mamaounakis, G. (2018). "Markov based transition probability geostatistics in groundwater applications: assumptions and limitations." Stoch Environ Res Risk Assess 32, 2129–2146, 10.1007/s00477-017-1504-y.

Li, D.-Q., Qi, X.-H., Cao, Z.-J., Tang, X.-S., Phoon, K.-K., and Zhou, C-B. (2016). "Evaluating slope stability uncertainty using coupled Markov chain." Computers and Geotechnics, 73: 72-82, 10.1016/j.compgeo.2015.11.021.

Liu, L., Cheng, Y., and Zhang, S., (2017). “Conditional random field reliability analysis of a cohesion-frictional slope.” Computers and Geotechnics, 82:173-186.

Mejia, K. H., and Dawson, E. M. (2006). “Earthquake Deconvolution for FLAC”. 4th International Symposium on Numerical Modeling in Geomechanics. Minneapolis, MN.

Montgomery, J., Boulanger, R. W., Armstrong, R. J., and Malvick, E. J. (2014). “Anisotropic Undrained Shear Strength Parameters for Nonlinear Deformation Analyses of Embankment Dams.” Geo-Congress 2014 Technical Papers.

Munter, S. K., Boulanger, R. W., Krage, C. P., and DeJong, J. T. (2017). “Evaluation of liquefaction-induced lateral spreading procedures for interbedded deposits: Cark Canal in the 1999 M7.5 Kocaeli earthquake.” Geotechnical Frontiers 2017, Seismic Performance and Liquefaction, Geotechnical Special Publication No. 281, T. L. Brandon and R. J. Valentine, eds., 254-266.

Paull, N. A., Boulanger, R. W., and DeJong, J. T. (2020). “Accounting for spatial variability in nonlinear dynamic analyses of embankment dams on liquefiable deposits.” Journal of Geotechnical and Geoenvironmental Engineering, ASCE, 2020.

Paull, N. A., Boulanger, R. W., and DeJong, J. T. (2020). “Nonlinear deformation analyses of embankments on a spatially variable liquefiable deposit using conditional random fields.” Geo-Congress 2020: Engineering, Monitoring, and Management of

Geotechnical Infrastructure. Geotechnical Special Publication 316, J. P. Hambleton, R. Makhnenko, and A. S. Budge (eds), ASCE, 1-9.

Pretell, R. A., Ziotopoulou, K., and Davis, C. (2020). “Numerical modeling of ground deformations at Balboa Blvd. in the Northridge 1994 Earthquake.” ASCE Journal of Geotechnical and Geoenvironmental Engineering.

Rennie, D., Driller, M., and Beaty, M. (2005). “Perris Dam Foundation Study.” California Department of Water Resources. Sacramento, CA.

Tang, W. H., and Halim, I. (1988). "Updating anomaly statistics – Multiple anomaly pieces." Journal of Engineering Mechanics, ASCE, 114(6): 1091-1096.

Tatone, F., Dawson, E. M., Hu, J., and Nguyen, D., (2018). “Application of SPT Rod Energy Loss to Liquefaction Evaluation of Deep Alluvium beneath an Earthfill Dam.” Geotechnical Earthquake Engineering and Soil Dynamics V. Houston, Tx.

URS (2009). “Site-Specific Seismic Hazard Analyses and Development of Time Histories for Perris Dam, California”. California Department of Water Resources. Sacramento, CA.

URS (2012). “Seismic Deformation Analysis with UBCSAND”. California Department of Water Resources. Sacramento, CA.

Wang, X., Wang, H., and Liang, R. Y. (2018). "A method for slope stability analysis considering subsurface stratigraphic uncertainty." Landslides, 15: 925-936, 10.1007/s10346-017-0925-5.

Wong, I., Thomas, P., Zachariasen, J., Hansen, L., Terra, F., and Lowenthal-Savy, D., (2009). “Site-Specific Seismic Hazard Analyses and Development of Time Histories for Perris Dam.” California Department of Water Resources. Sacramento, CA.

Table 1: Properties for T-PROGS realizations.

Soil properties from site investigation used in TPROGS	Holocene Alluvium	Pleistocene Alluvium
Clay sill (%)	46.1	39.5
Clay vertical mean length (m)	1.0	2.0
Clay along channel mean length (m)	25.0	25.0
Clay cross channel mean length (m)	10.0	10.0
Nonliquefiable sand sill (%)	27.6	51.3
Nonliquefiable sand vertical mean length (m)	1.0	4.0
Nonliquefiable sand along channel mean length (m)	25.0	25.0
Nonliquefiable sand cross channel mean length (m)	10.0	10.0
Liquefiable sand sill (%)	26.3	9.2
Liquefiable sand vertical mean length (m)	1.0	1.0
Liquefiable sand along channel mean length (m)	25.0	25.0
Liquefiable sand cross channel mean length (m)	10.0	5.0

Table 2: Alluvial constitutive model properties for baseline models.

Soil properties from site investigation used in constitutive models	Holocene Alluvium	Pleistocene Alluvium
Clay constitutive model	PM4Silt	PM4Silt
Clay undrained shear strength ratio, $S_{u,cs,eq}/\sigma'_{vc}$	0.3	0.3
Clay shear modulus coefficient, G_o	3272	3272
Clay contraction rate parameter, h_{po}	5.0	6.0
Nonliquefiable sand constitutive model	PM4Sand	PM4Sand
Nonliquefiable sand $(N_1)_{60,cs}$	36	39
Nonliquefiable sand relative density, D_R (%)	85.7	89.2
Nonliquefiable sand shear modulus coefficient, G_o	3272	3272
Nonliquefiable sand contraction rate parameter, h_{po}	0.07	0.007
Liquefiable sand constitutive model	PM4Sand	PM4Sand
Liquefiable sand $(N_1)_{60,cs}$	14	16
Liquefiable sand relative density, D_R	53.5	57.1
Liquefiable sand shear modulus coefficient, G_o	2203	2203
Liquefiable sand contraction rate parameter, h_{po}	0.17	0.06

1002

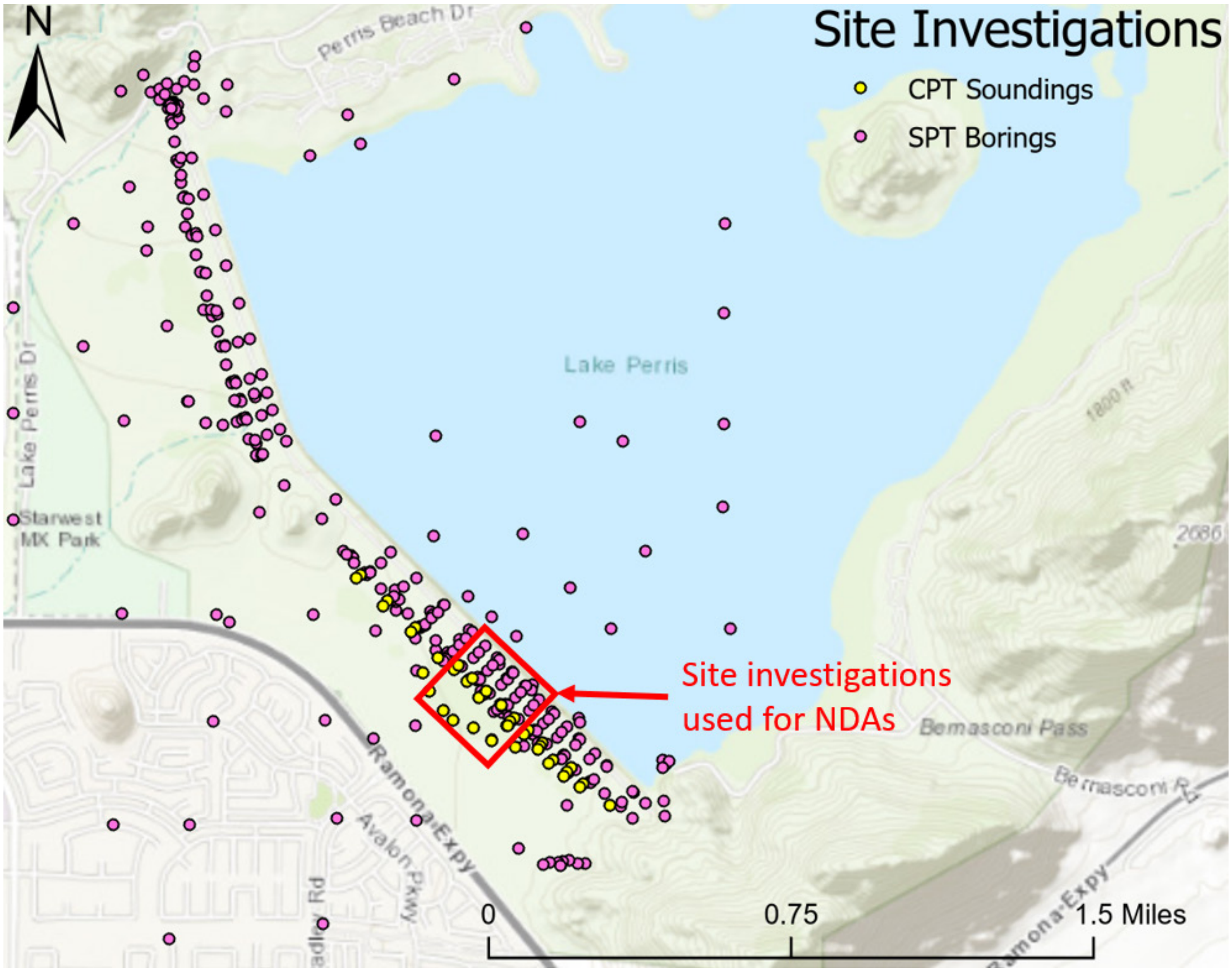

1003 Fig. 1: Map of Perris Dam site investigation locations.

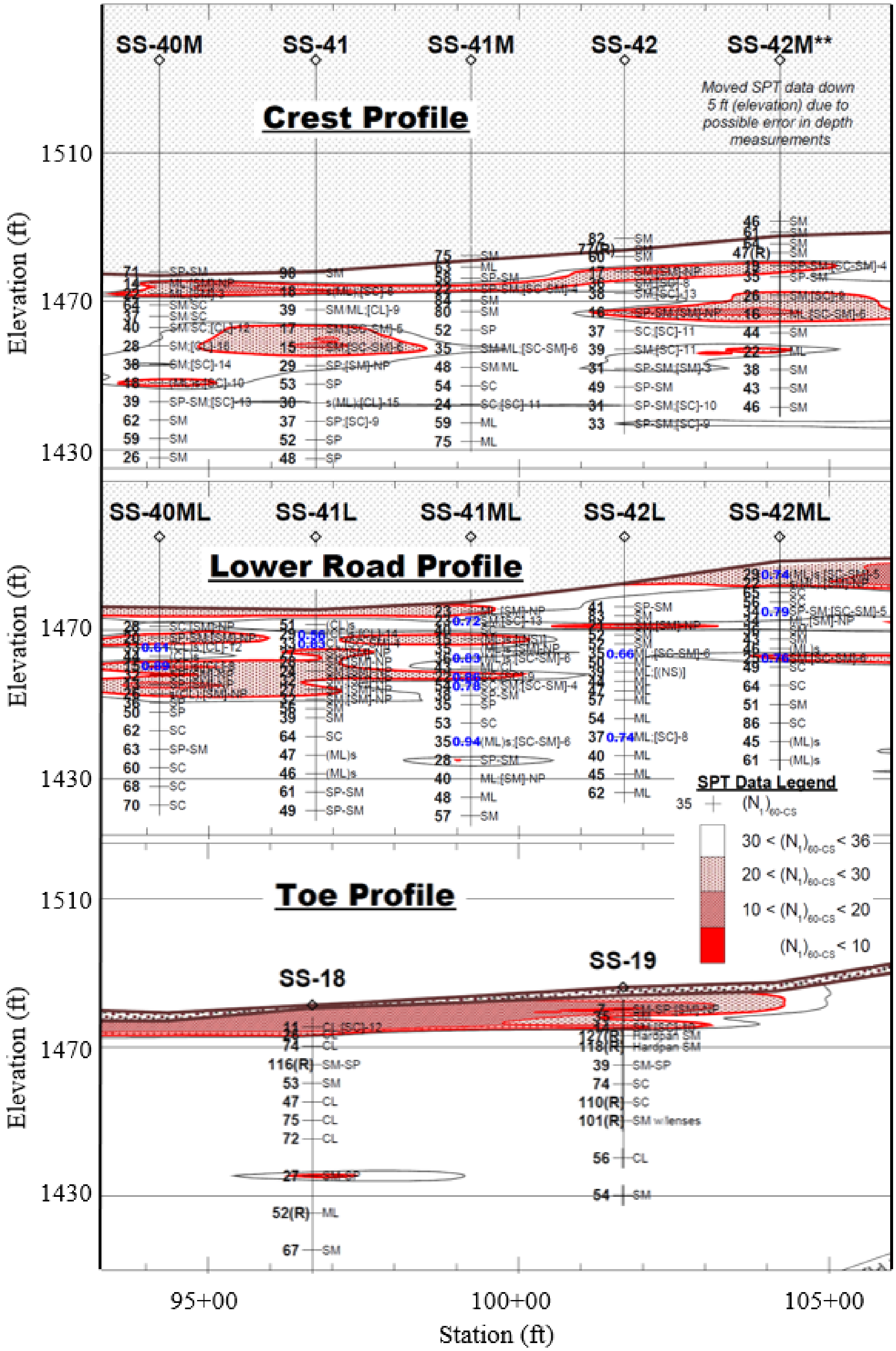

Fig. 2: Longitudinal profiles of the Perris Dam left reach along the approximate extents of the NDA models with SPT data (Modified from DWR, 2015).

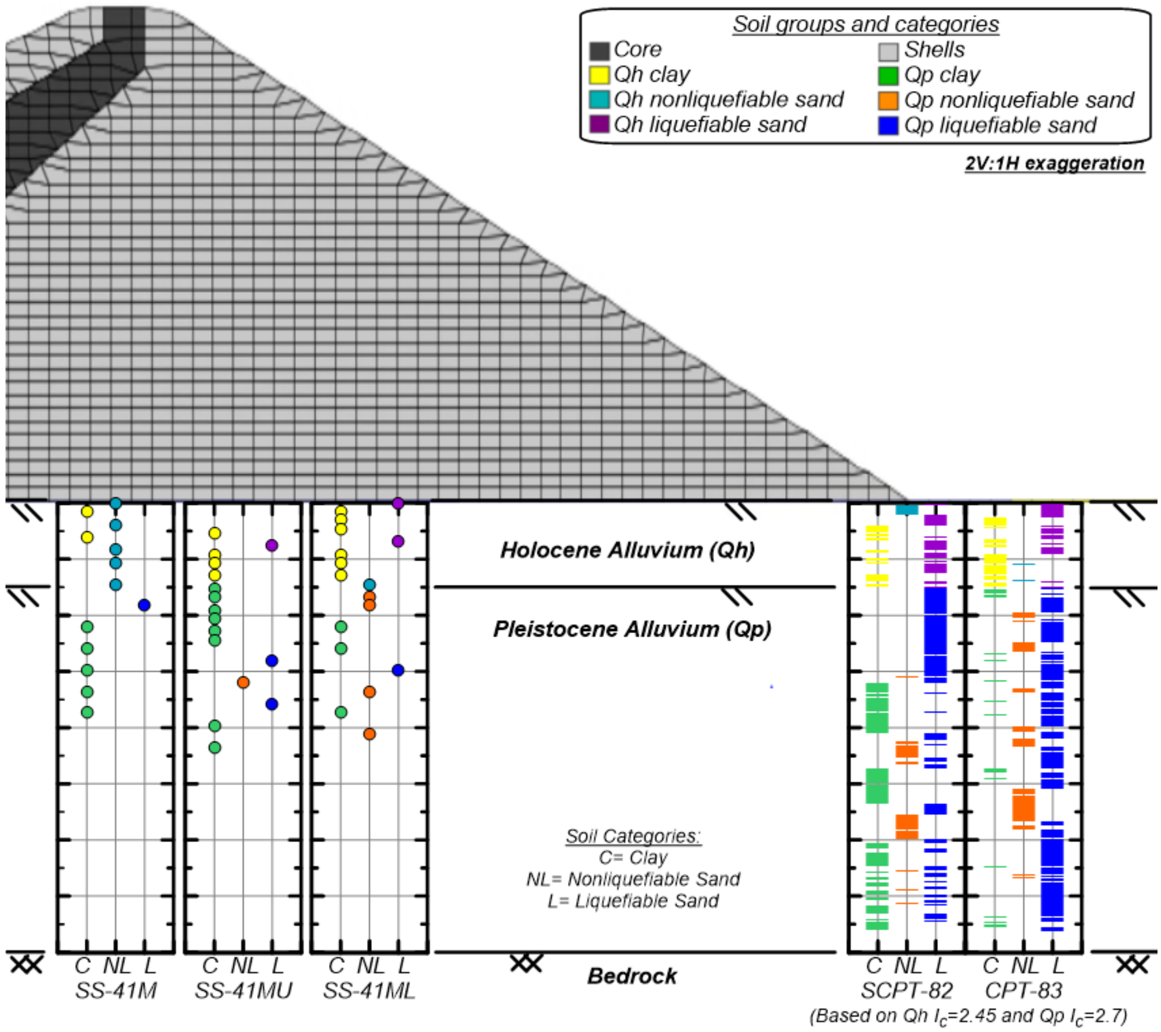

Fig. 3: Cross-section of Perris Dam at STA 99+20 with soil groups assessed based on the site investigation data.

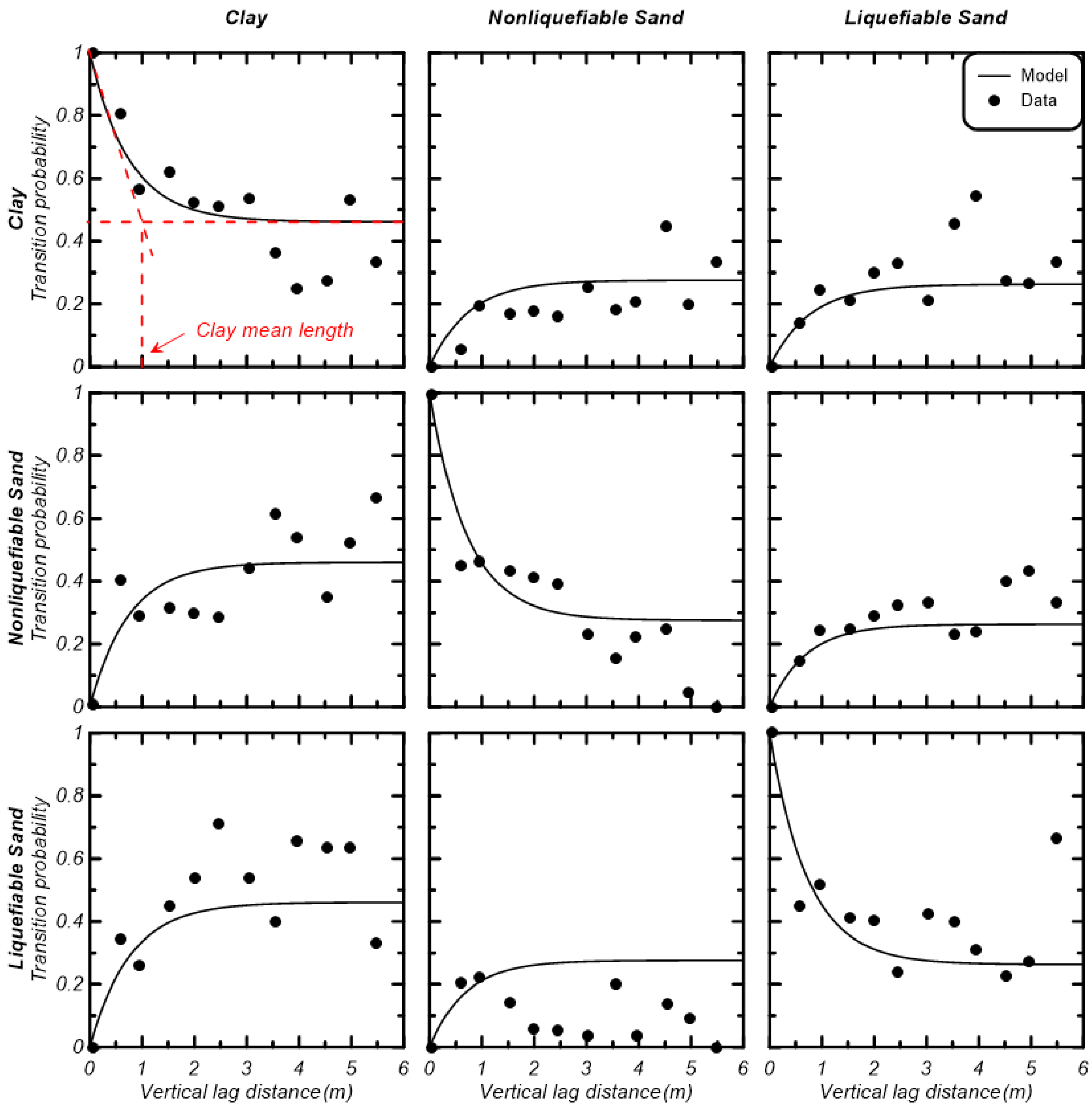

1011
1012 Fig. 4: Vertical transition probability matrix for either the Holocene Alluvium baseline
1013 cases.

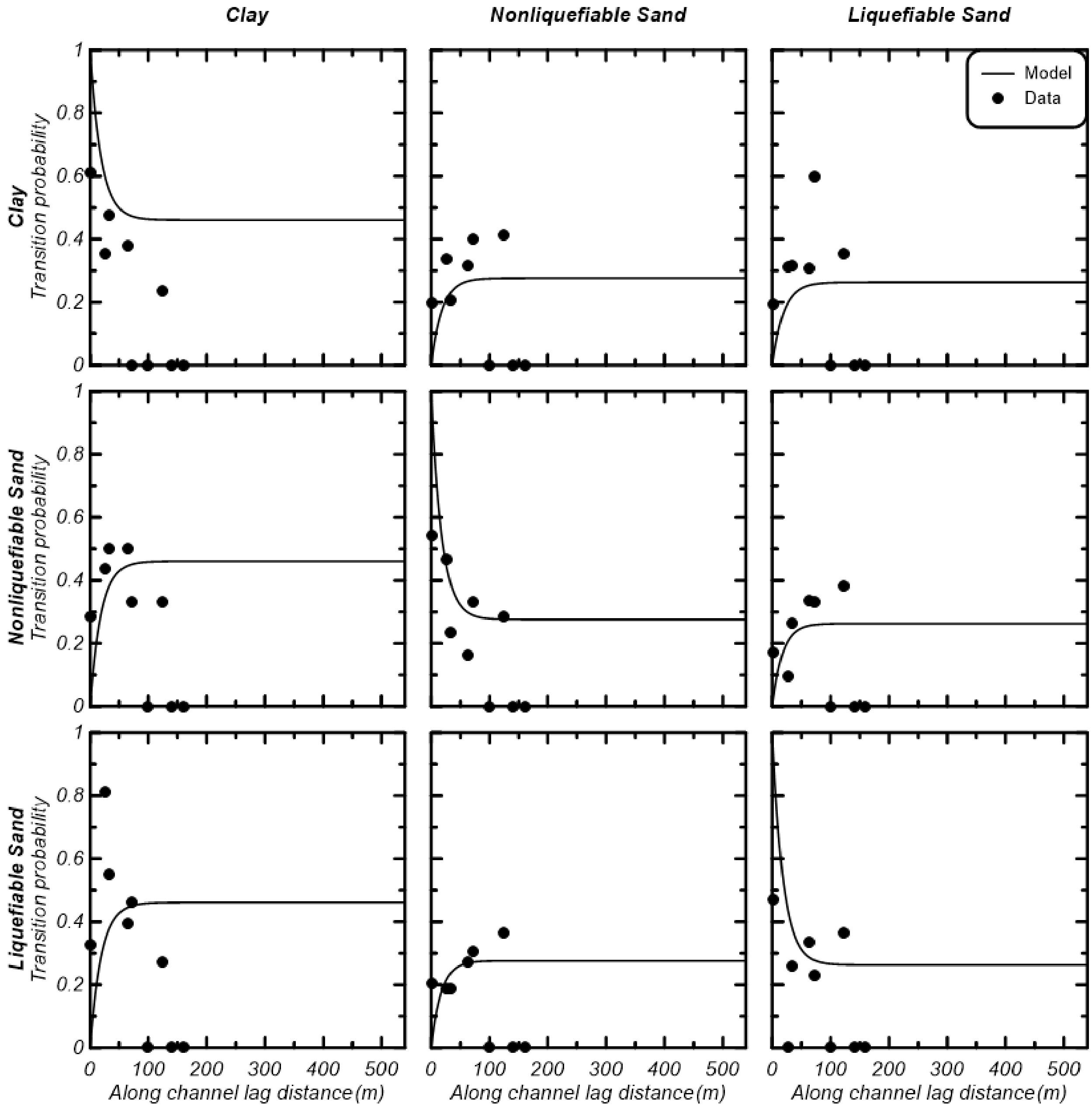

1014
1015 Fig. 5: Along channel transition probability matrix for either the Holocene Alluvium
1016 baseline cases.

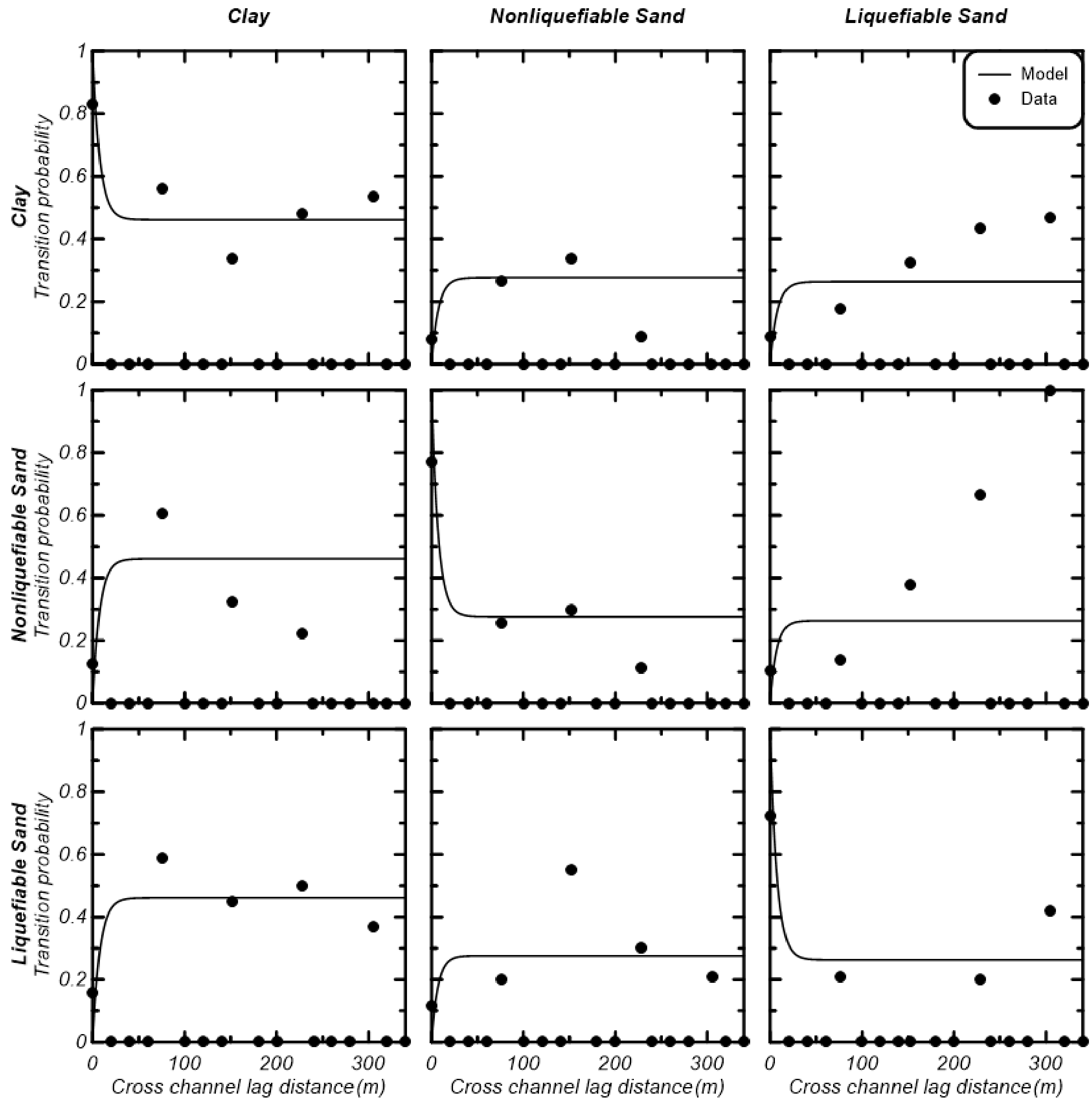

Fig. 6: Cross channel transition probability matrix for either the Holocene Alluvium baseline cases.

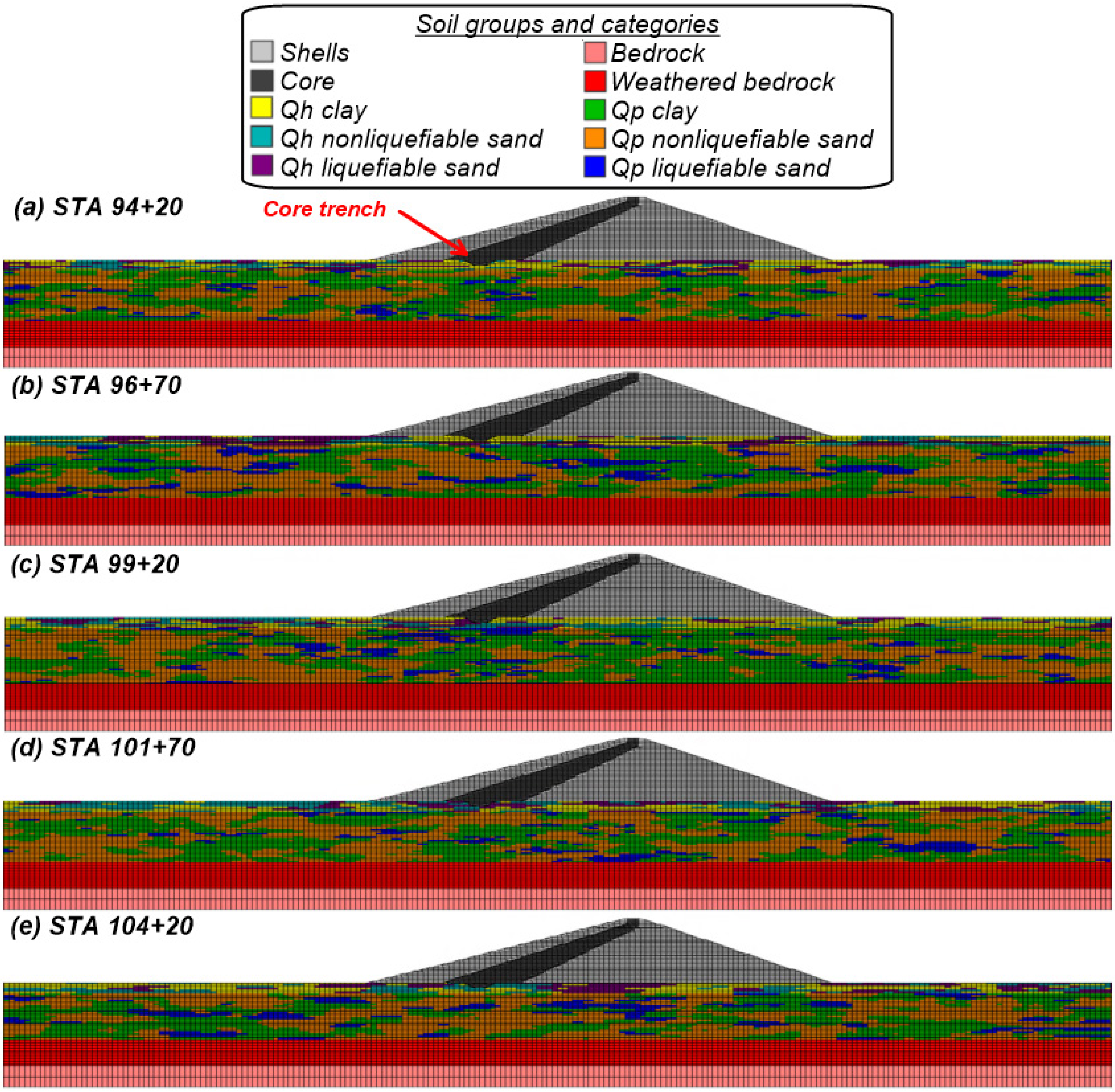

1020
1021 Fig. 7: Perris Dam NDA cross sections showing the soil groups and categories for (a)
1022 STA 94+20, (b) STA 96+70, (c) STA 99+20, (d) STA 101+70, (e) STA 104+20.

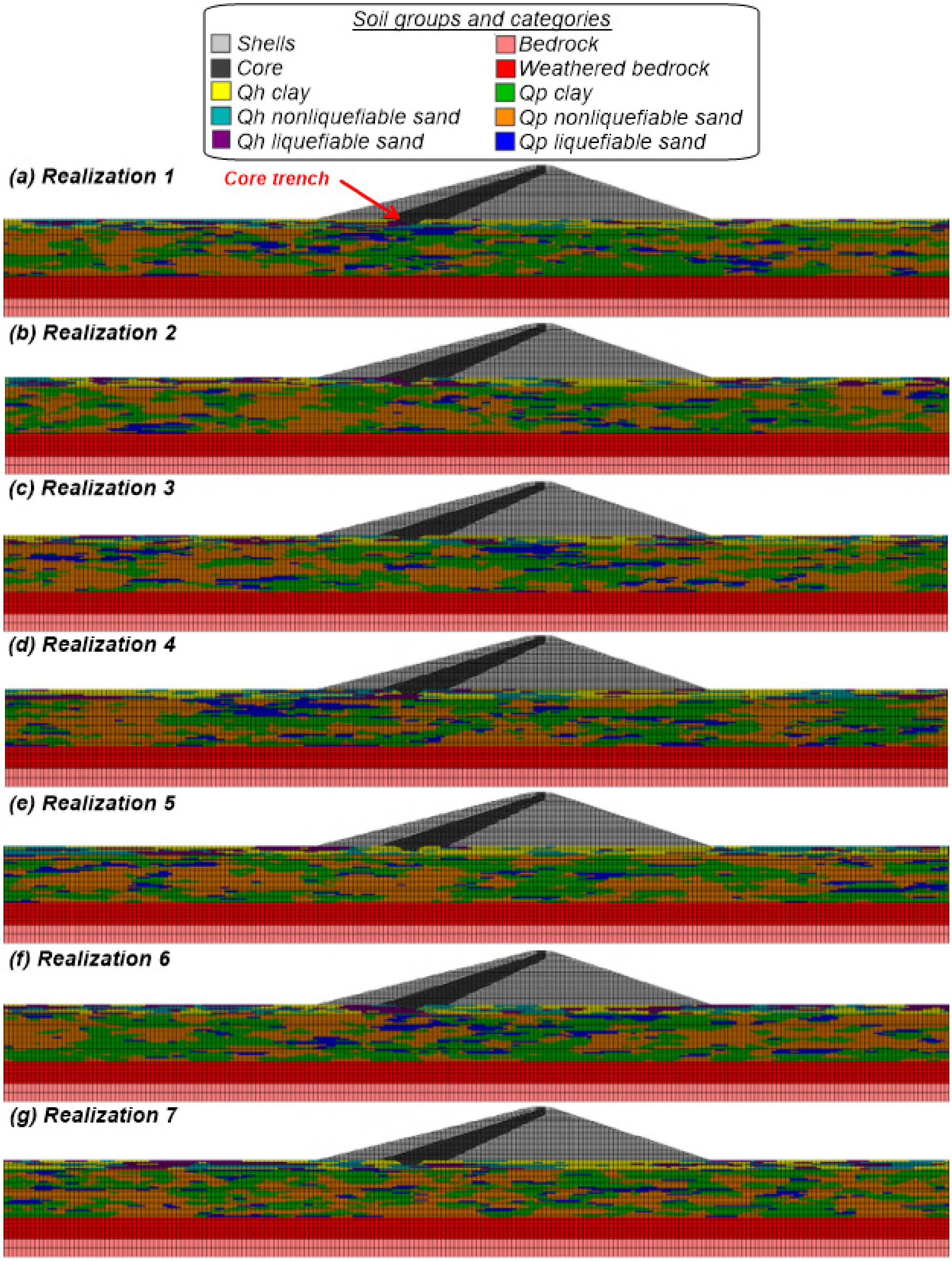
Soil groups and categories
Shells
Core
Qh clay
Qh nonliquefiable sand
Qh liquefiable sand
Bedrock
Weathered bedrock
Qp clay
Qp nonliquefiable sand
Qp liquefiable sand
(a) Realization 1
Core trench
(b) Realization 2
(c) Realization 3
(d) Realization 4
(e) Realization 5
(f) Realization 6
(g) Realization 7

1023

Fig. 8: Perris Dam NDA at STA 99+20 showing the soil groups and categories with alluvium represented with (a) realization 1, (b) realization 2, (c) realization 3, (d) realization 4, (e) realization 5, (f) realization 6, (g) realization 7.

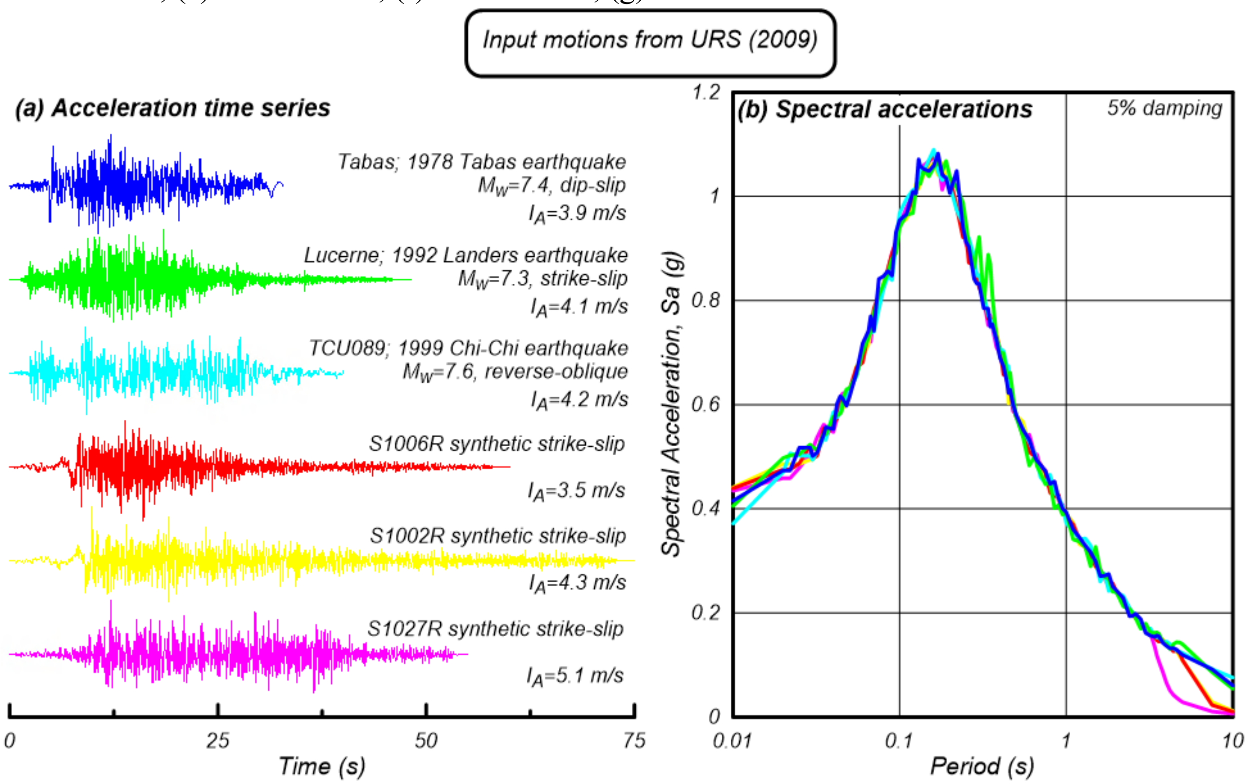

Fig. 9: (a) Acceleration time series and (b) spectral accelerations for input motions obtained from URS (2009).

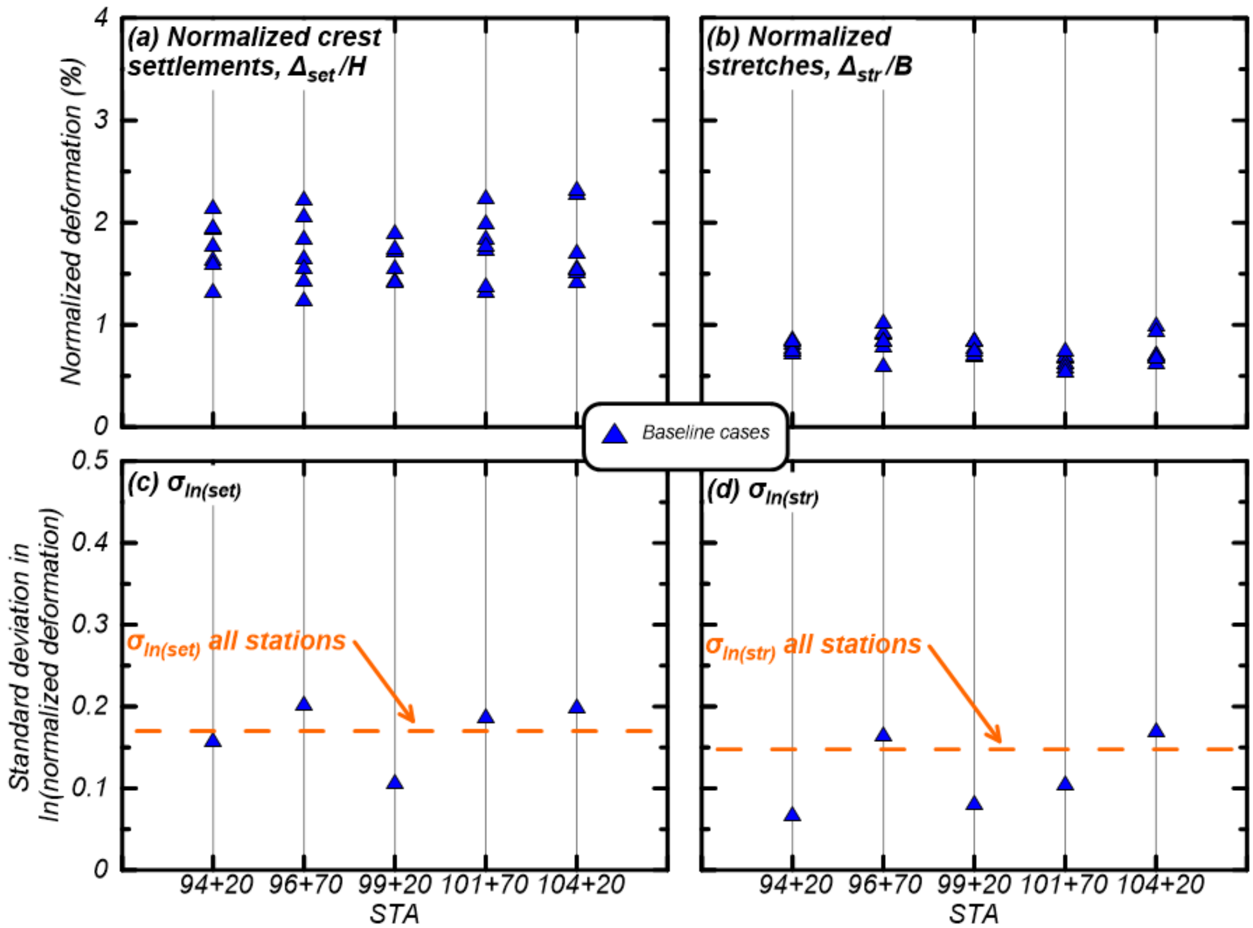

Fig. 10: (a) Normalized crest settlements (Δ_{set}/H), (b) Normalized embankment stretches (Δ_{str}/B), (c) standard deviations of ln(normalized crest settlements), and (d) standard deviations of ln(normalized embankment stretches) for cross sections at different sections along Perris Dam subjected to the Tabas motion for the baseline cases.

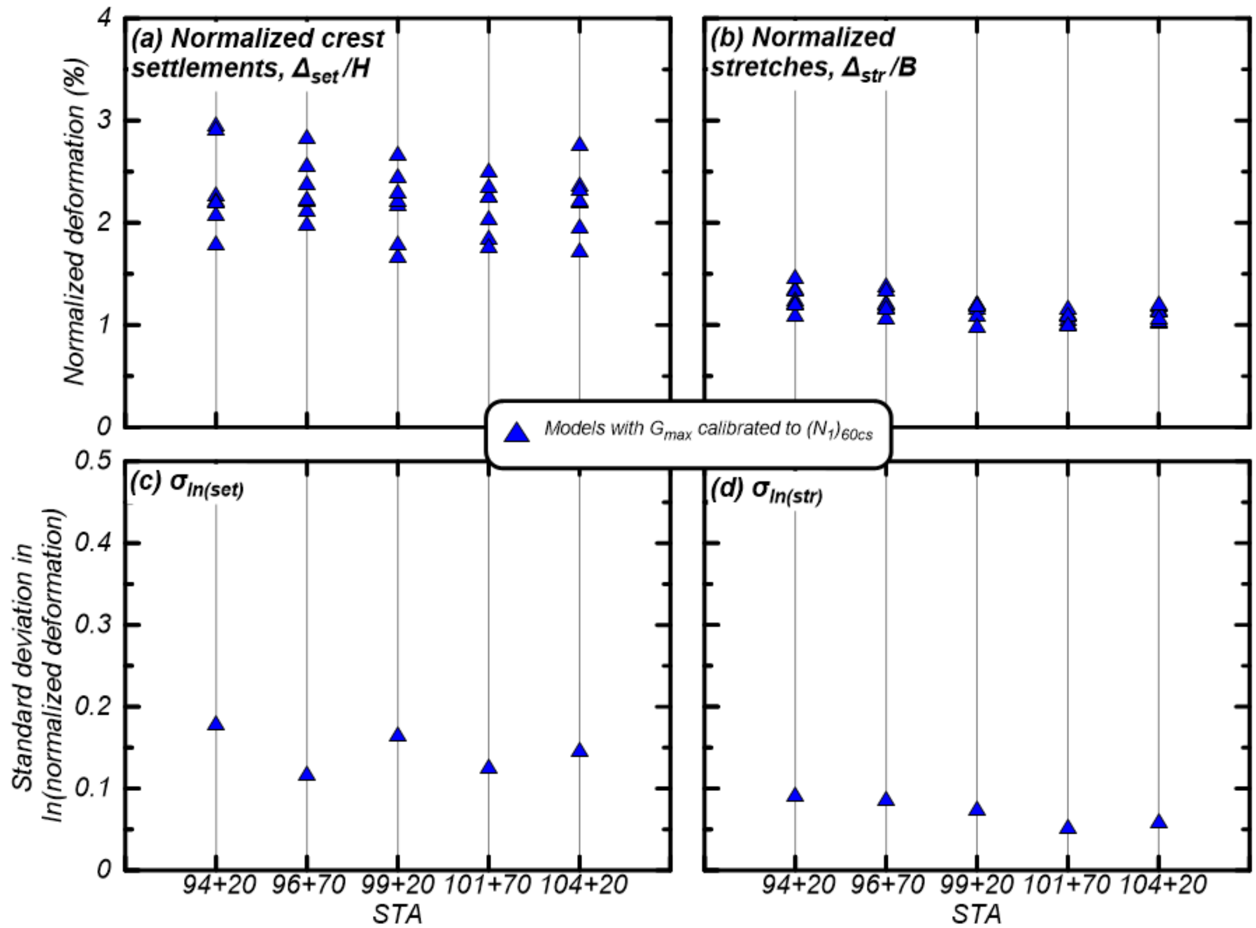

Fig. 11: (a) Normalized crest settlements (Δ_{set}/H), (b) Normalized embankment stretches (Δ_{str}/B), (c) standard deviations of ln(normalized crest settlements) and (d) standard deviations of ln(normalized embankment stretches) for cross sections at different sections along Perris Dam subjected to the Tabas motion for the cases calibrated without including the effects of cementation.

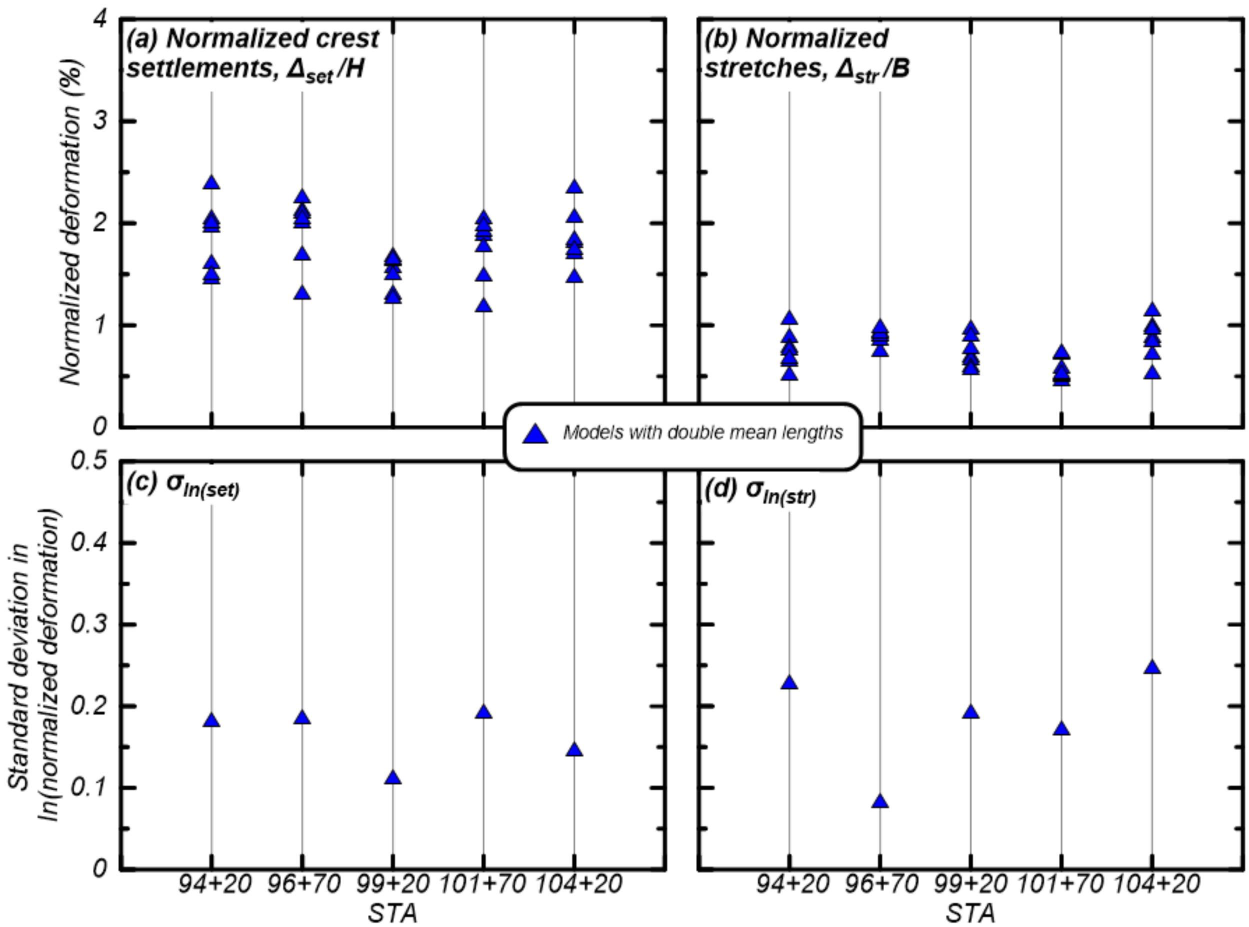

Fig. 12: (a) Normalized crest settlements (Δ_{set}/H), (b) Normalized embankment stretches (Δ_{str}/B), (c) standard deviations of ln(normalized crest settlements) and (d) standard deviations of ln(normalized embankment stretches) for cross sections at different sections along Perris Dam subjected to the Tabas motion for the baseline cases with all mean lengths doubled.

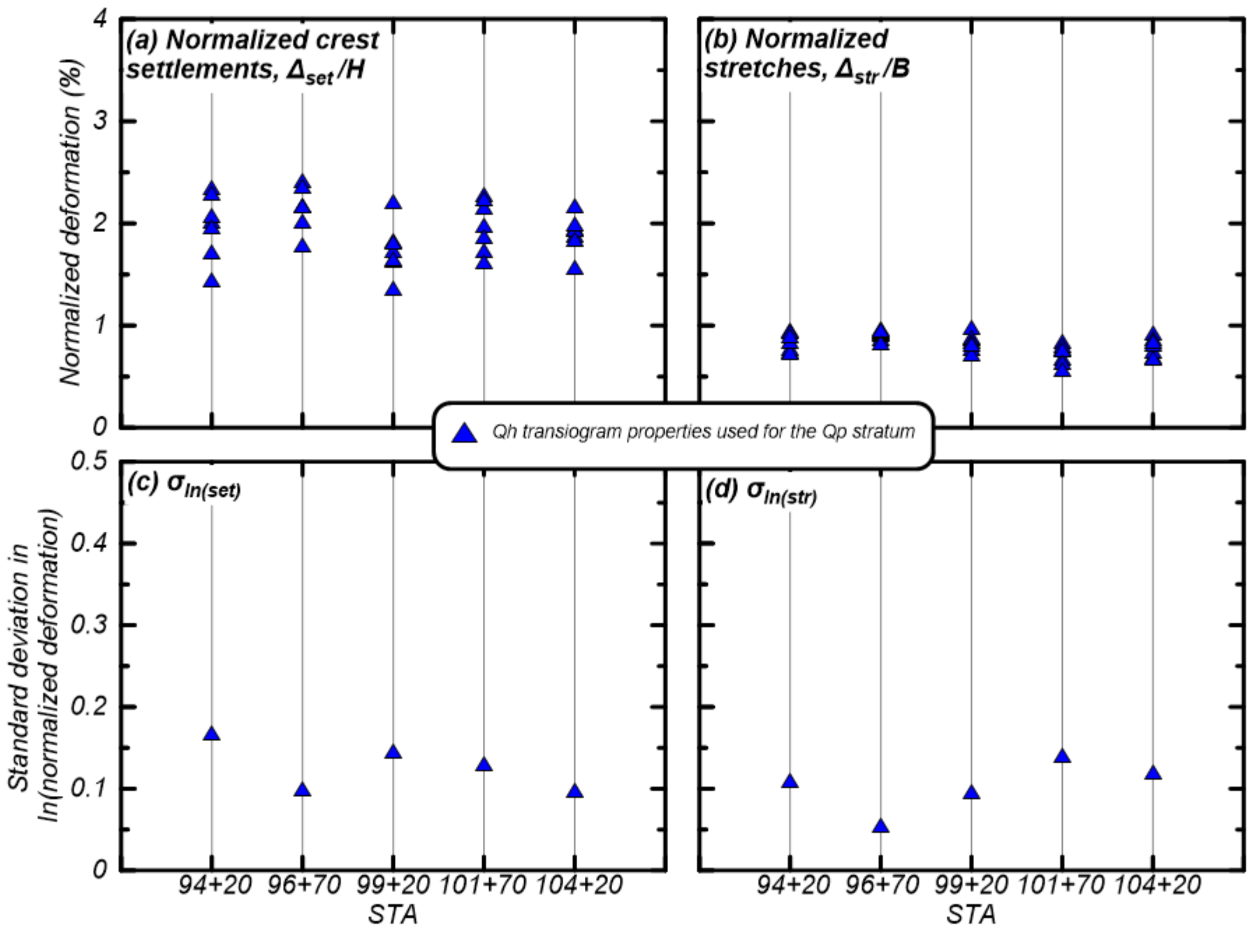

Fig. 13: (a) Normalized crest settlements (Δ_{set}/H), (b) Normalized embankment stretches (Δ_{str}/B), (c) standard deviations of ln(normalized crest settlements) and (d) standard deviations of ln(normalized embankment stretches) for cross sections at different sections along Perris Dam subjected to the Tabas motion with the Holocene Alluvium soil group sills and mean lengths used for the Pleistocene Alluvium.

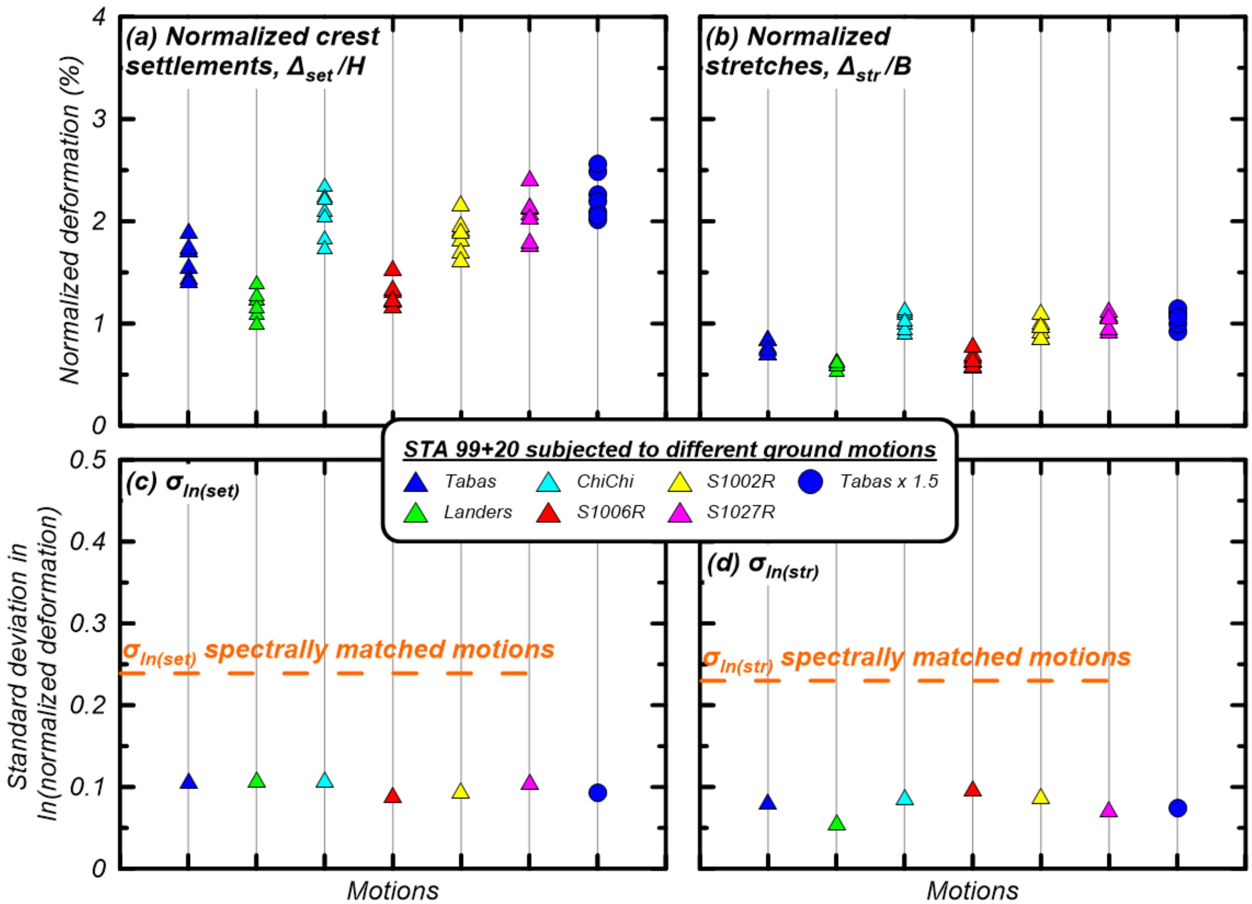

Fig. 14: (a) Normalized crest settlements (Δ_{set}/H), (b) Normalized embankment stretches (Δ_{str}/B), (c) standard deviations of ln(normalized crest settlements) and (d) standard deviations of ln(normalized embankment stretches) for the cross sections at STA 99+20 along Perris Dam subjected to the different motions.

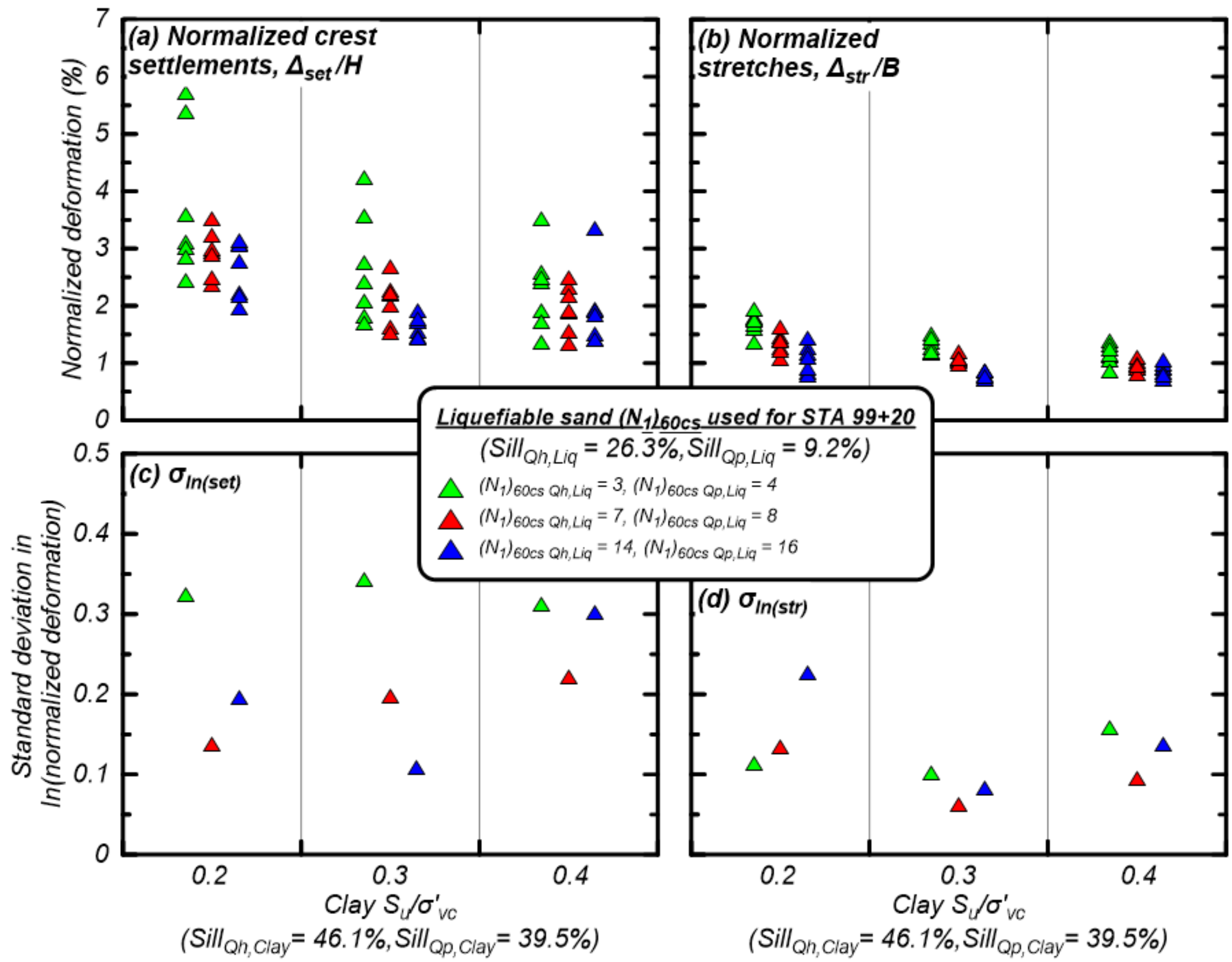

Fig. 15: (a) Normalized crest settlements (Δ_{set}/H), (b) Normalized embankment stretches (Δ_{str}/B), (c) standard deviations of ln(normalized crest settlements) and (d) standard deviations of ln(normalized embankment stretches) for cross sections at different sections along Perris Dam subjected to the Tabas motion for the baseline cases with different assumed property values for each alluvial soil group.

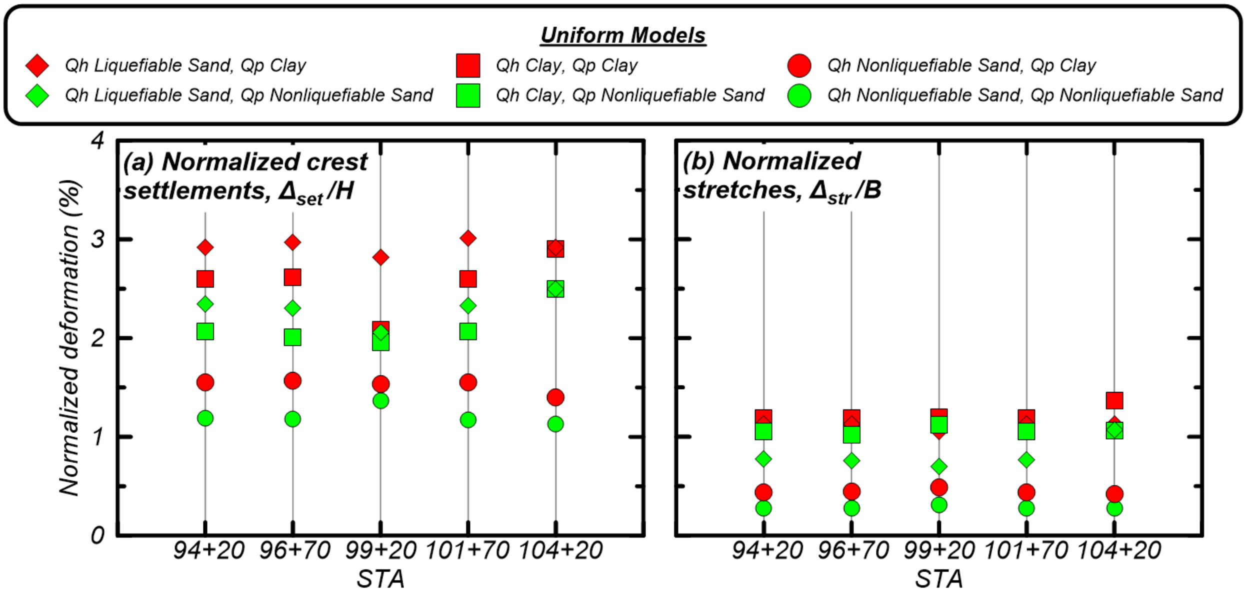

Fig. 16: (a) Normalized crest settlements (Δ_{set}/H), and (b) Normalized embankment stretches (Δ_{str}/B) for cross sections at different sections along Perris Dam subjected to the Tabas motion for different combinations of uniform model assumptions.

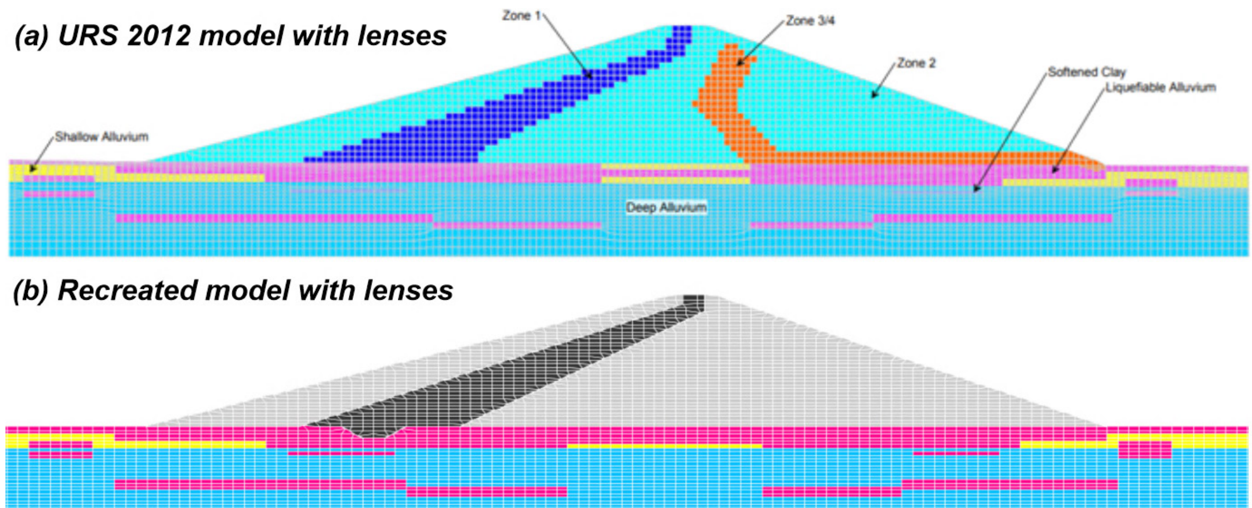

Fig. 17: Undeformed (a) URS 2012 model with deterministic embedded lenses and (b) recreated model with deterministic embedded lenses.

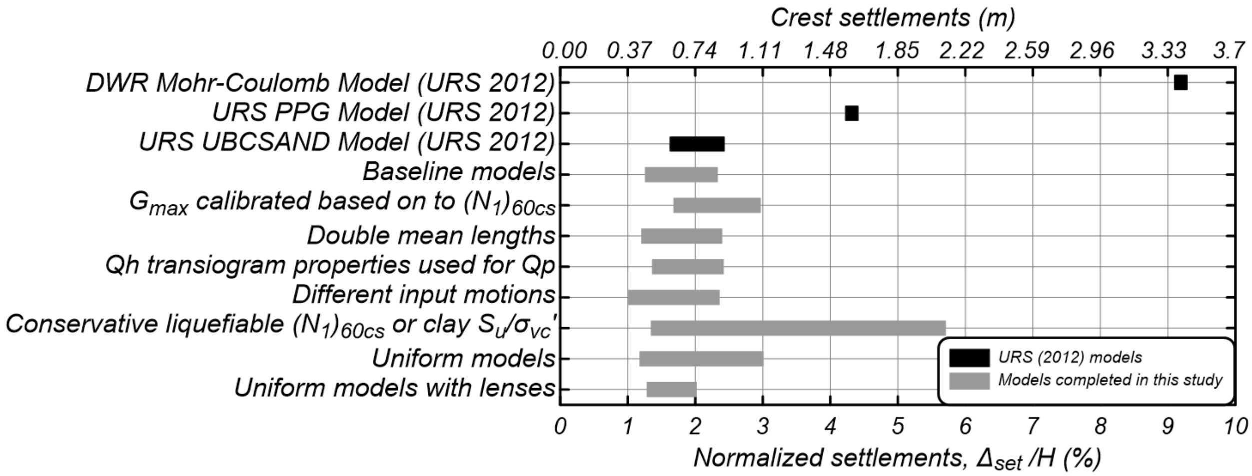

Fig. 18: A summary of normalized crest settlements for models completed in URS (2012) and all models conducted in this study.

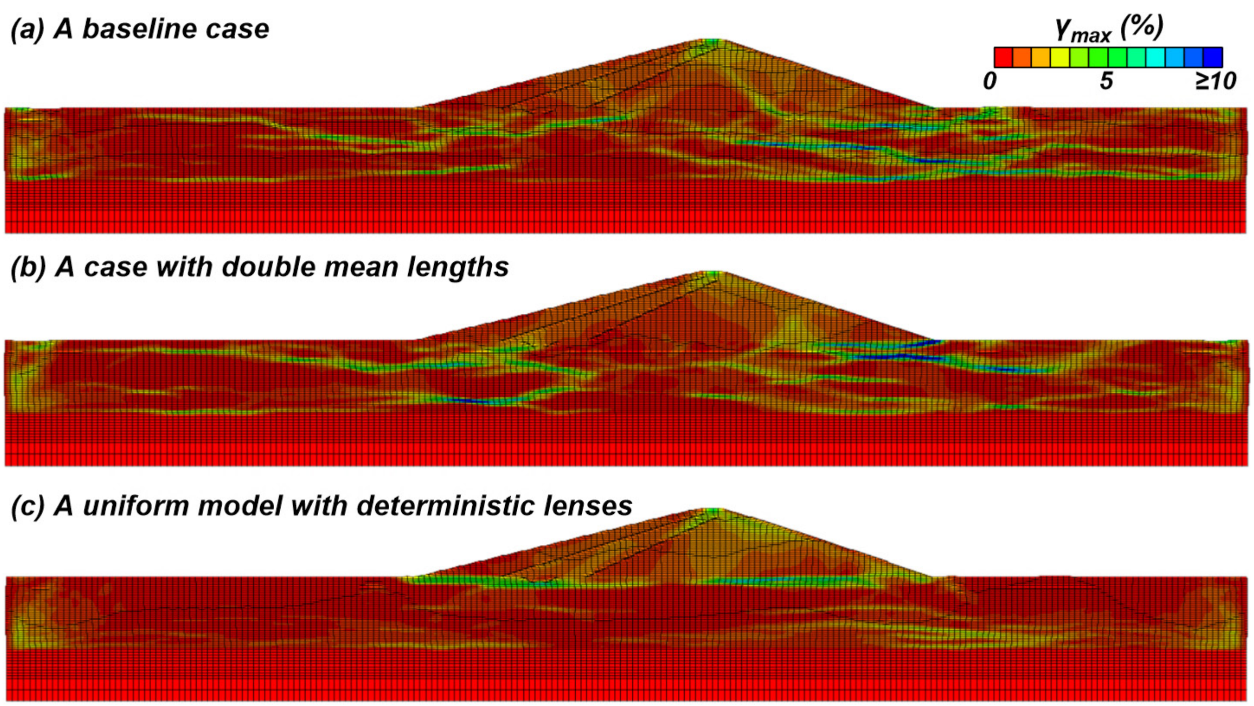

Fig. 19: Shear strains for (a) a baseline case, (b) a case with double mean lengths, and (c) a uniform model with deterministic embedded lenses.